ATTACHMENT 4

CDI Report No. 04-09P

Methodology to Determine Unsteady Pressure Loading on Components in Reactor Steam Domes, Revision 5

(Non-Proprietary)

AFFIDAVIT

Re: "Methodology to Determine Unsteady Pressure Loading on Components in Reactor Steam Domes," Presentation prepared by Continuum Dynamics, Inc. for Exelon Generation LLC, 25 January 2005; and
"Methodology to Determine Unsteady Pressure Loading on Components in Reactor Steam Domes," C.D.I. Report No. 04-09P Rev. 5, prepared by Continuum Dynamics, Inc., dated January 2005.

I, Alan J. Bilanin, being duly sworn, depose and state as follows:

1. I hold the position of President and Senior Associate of Continuum Dynamics, Inc. (hereinafter referred to as C.D.I.), and I am authorized to make the request for withholding from Public Record the Information contained in the documents described in Paragraph 2. This Affidavit is submitted to the Nuclear Regulatory Commission (NRC) pursuant to 10 CFR 2.390(a)(4) based on the fact that the attached information consists of trade secret(s) of C.D.I. and that the NRC will receive the information from C.D.I. under privilege and in confidence.

2. The Information sought to be withheld, is contained in the presentation entitled "Methodology to Determine Unsteady Pressure Loading on Components in Reactor Steam Domes," prepared by Continuum Dynamics, Inc. for Exelon Generation LLC, dated 25 January 2005 and C.D.I. Report No. 04-09P, Rev. 5, entitled "Methodology to Determine Unsteady Pressure Loading on Components in Reactor Steam Domes," prepared by Continuum Dynamics, Inc., dated January 2005 transmitted to Keith Moser, Exelon in email dated January 21, 2005.

3. The Information summarizes:

   (a) a process or method, including supporting data and analysis, where prevention of its use by C.D.I.'s competitors without license from C.D.I. constitutes a competitive advantage over other companies;
   (b) Information which, if used by a competitor, would reduce his expenditure of resources or improve his competitive position in the design, manufacture, shipment, installation, assurance of quality, or licensing of a similar product;
   (c) Information which discloses patentable subject matter for which it may be desirable to obtain patent protection.

   The information sought to be withheld is considered to be proprietary for the reasons set forth in paragraphs 3(a), 3(b) and 3(c) above.

4. The Information has been held in confidence by C.D.I., its owner. The Information has consistently been held in confidence by C.D.I. and no public disclosure has been made and it is not available to the public. All disclosures to third parties, which have been limited, have been made pursuant to the terms and conditions contained in C.D.I.'s Proprietary Information Exchange Agreement which must be fully executed prior to disclosure.

5. The Information is a type customarily held in confidence by C.D.I. and there is a rational basis therefore. The Information is a type, which C.D.I. considers trade secret and is held in confidence by C.D.I. because it constitutes a source of competitive advantage in the competition and performance of such work in the industry. Public disclosure of the Information is likely to cause substantial harm to C.D.I.'s competitive position and foreclose or reduce the availability of profit-making opportunities.

I declare under penalty of perjury that the foregoing affidavit and the matters stated therein are true and correct to be the best of my knowledge, information and belief.

Executed on this 31st day of January 2005.

Alan J. Bilanin
Continuum Dynamics, Inc.

Subscribed and sworn before me this day: Jan 31, 2005

Barbara A. Agans, Notary Public

BARBARA A. AGANS
NOTARY PUBLIC OF NEW JERSEY
MY COMM. EXPIRES MAY 6, 2007

C.D.I. Report No. 04-09P

Methodology to Determine Unsteady Pressure Loading on Components in Reactor Steam Domes

Revision 5

Prepared by:

Continuum Dynamics, Inc.
34 Lexington Avenue
Ewing, NJ 08618

January 2005

Table of Contents

1. Introduction

Estimation of the magnitude of the unsteady pressure loads on components inside a reactor steam dome is complicated by the environment in the dome itself. It is desirable to develop a loads transfer methodology to infer the fluctuating pressure field from existing in-plant measurement transducers, provided that it can be demonstrated that the methodology (algorithm) is robust and accurate. This report documents an algorithm that uses well-established analytical methods to compute the unsteady pressure loading in the steam dome using several simultaneous measurements of pressure in the steam supply system. The model is validated with data taken in the Quad Cities Unit 2 plant by comparing predictions of the fluctuating pressure at a location in the B main steam line with inferred data hoop stress pressure measurements.

2. Observations and Scaling Considerations

Previous analysis of main steam line pressure data [1-3] indicates the presence of discrete frequencies, which suggests that deterministic mechanisms are active in the steam delivery system. Furthermore, these mechanisms are power/flow rate sensitive. Most flow-induced vibration mechanisms that involve unsteady shear layer oscillations scale with dynamic pressure at constant Mach number. For power uprate in boiling water reactor (BWR) plants, system pressures do not change, and increased power is achieved by increasing steam flow velocity in the system. This increase in velocity results in an increase in both the Mach number and dynamic pressure, which scales with the velocity and velocity squared, respectively.

A simple but relevant example illustrates the difficulty in estimating the fluctuating pressures in a complex system. Figure 2-1 illustrates the scaling of the unsteady pressure due to flow over a dead-ended branch line. Data from [4] suggests that the root mean square pressure scales with the dynamic pressure $q = 1/2\ \rho U^2$ at constant Mach number (U/a), where

U is the flow velocity over the branch line

ρ is the fluid density

a is the acoustic speed in the fluid

L is the branch line length

d is the branch line diameter

This scaling can be directly obtained from a scaling analysis. From Figure 2-1, it is apparent that only when $ad/4LU \approx 0.44$ do the pressure fluctuations scale as U^2. For sufficiently low and high velocities, pressure fluctuations disappear.

In a system with many junctions and branch lines of various lengths and diameters, it is clear that a simple "back of the envelope" analysis is not achievable to estimate the unsteady loads as a function of reactor power. For this reason, a methodology is

developed that uses measured in-plant data to infer unsteady loading on the dryer (or any internal component) as a function of reactor power.

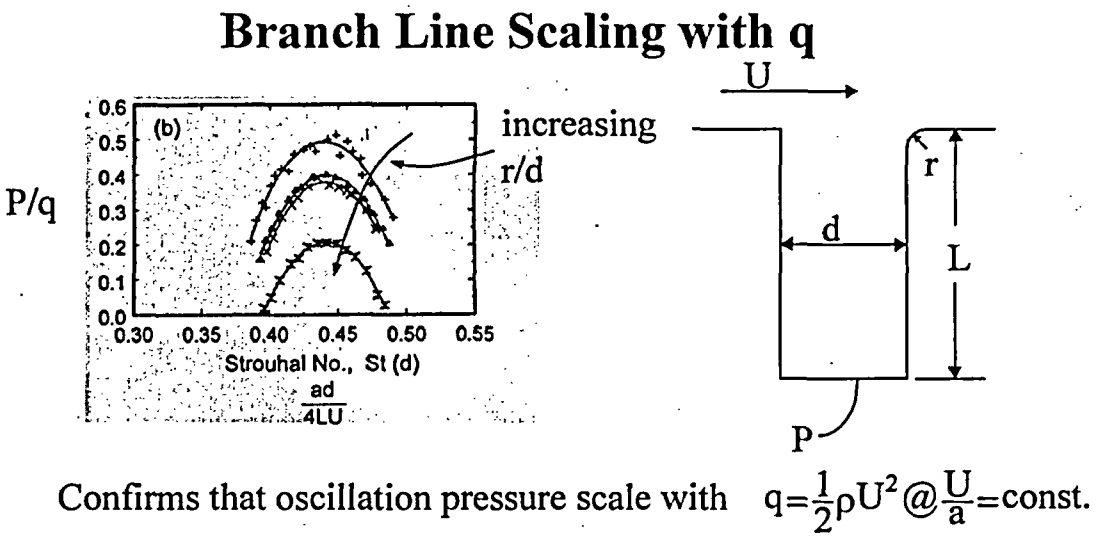

Figure 2-1 Oscillation in a stagnant branch line.

3. Methodology Formulation

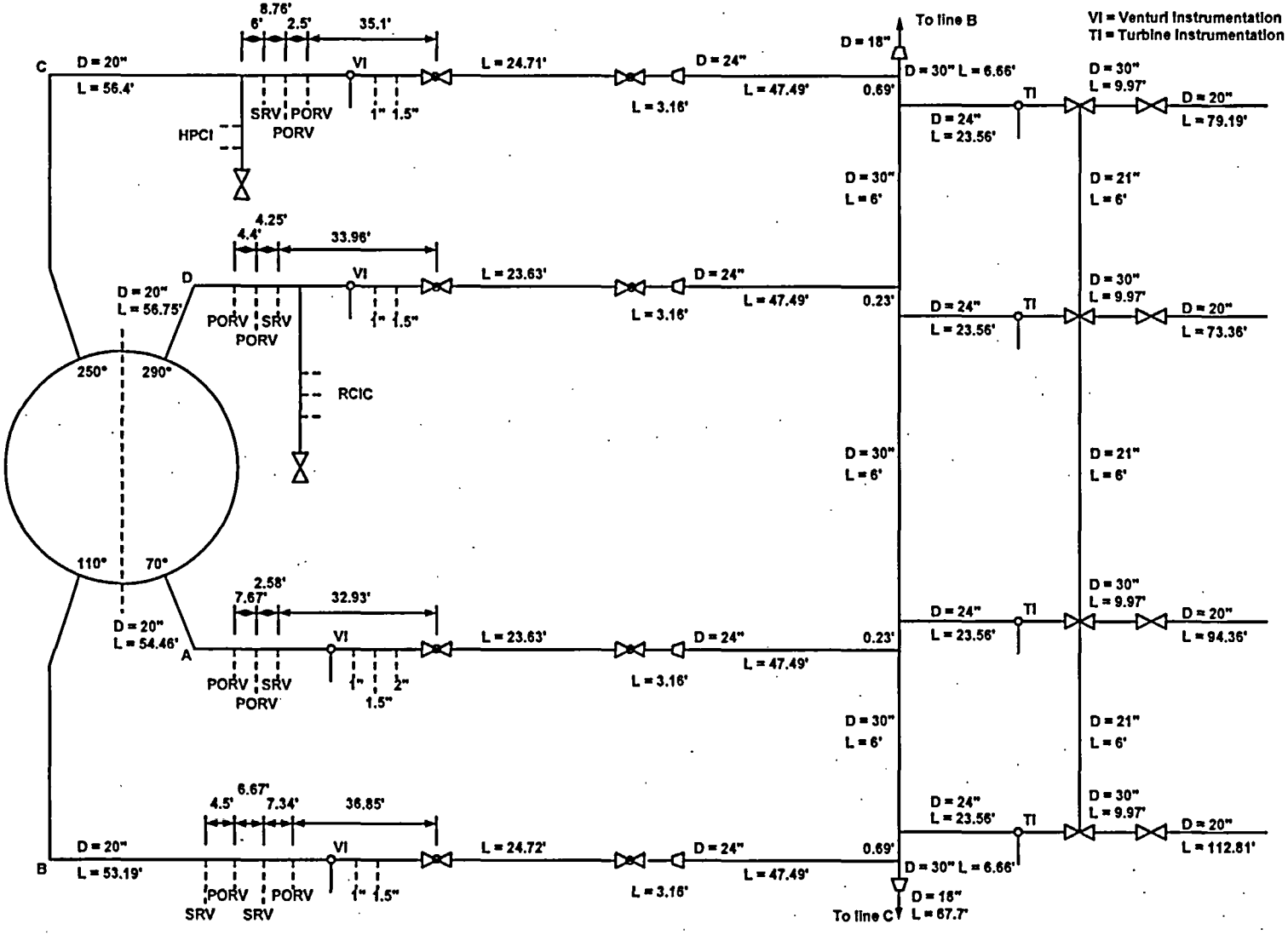

Figure 3-1 Piping geometry used in the acoustic circuit analysis for Quad Cities Unit 2 (QC2).

It is desired to develop an analysis where the pressure field is computed correctly to the order of the Mach number, which is common for hydrodynamic analysis. The hydrodynamic pressure field is typically of the order of Mach number squared. In the steam dome where the Mach number is small, the convective wave equation reduces to the standard wave equation:

$$\frac{1}{a^2}\frac{\partial^2 P}{\partial t^2} - \nabla^2 P = 0$$

In the steam lines where the flow is essentially one-dimensional, the pressure satisfies the following:

$$\frac{1}{a^2}\frac{D^2 P}{Dt^2} - \frac{\partial^2 P}{\partial x^2} = 0$$

where $\frac{D}{Dt} = \frac{\partial}{\partial t} + U\frac{\partial}{\partial x}$, and U is the velocity in the main steam line.

†

Source region II is well known and exists when a shear flow passes over a dead ended branch line [4, 5]. It is well established that if the velocity over the branch line is $U \approx 0.55 da/L$, the branch line is excited at the quarter standing acoustic wave in the branch line (also referred to as the first organ pipe mode). Acoustic oscillations exist at a frequency of $a/4L$ and radiate into the flowing system. This mechanism is postulated to occur at the turbine equalizer lines located upstream of the control valves.

† This acoustic excitation mechanism exists in other physical systems, most notably a children's toy consisting of a corrugated tube approximately 3 feet in length and open on both ends. When spun while holding one end, the tube "sings" at a fixed tone corresponding to the 1/4 standing wave frequency of the tube. The acoustic forcing is supplied by unsteady vortex shedding from the lip of the tube, which periodically perturbs the vena contracta and corresponding head loss of the air entering the tube.

The latter measurement is converted to an internal pressure, which is used for model validation. In total, eleven independent measurements are available to deduce the pressure fluctuations in the steam dome for this specific example. However, although sources have been assumed at geometric locations, it is not apparent that analyses of test data would show that some of these sources are in fact negligible.

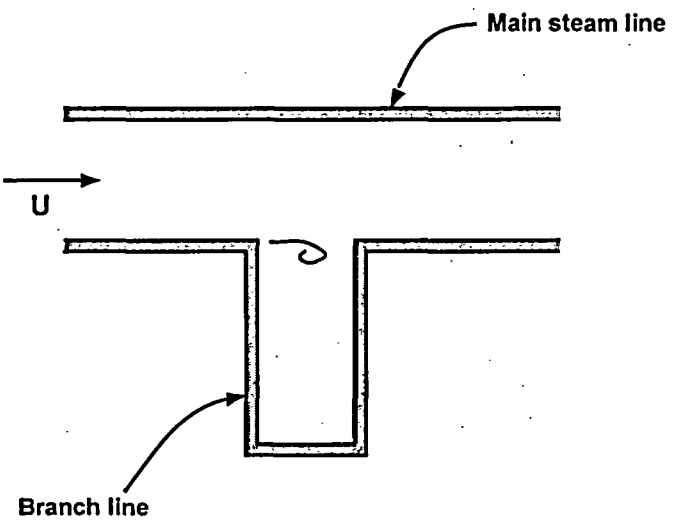

Figure 3-2 Conceptualization of source regions.

4. Component Models

In this section, models used to represent the dynamics of specific component in the steam supply system are described.

4.1 Steam Dome

A cross-section of the steam dome and steam dryer is shown in Figure 4-1 (a schematic top view of the steam dryer is shown in Figure 6.2). Dimensions corresponding the QC2 example, as verified in [6], are also indicated. The unsteady pressure field is determined by periodic solution of the wave equation, since Mach numbers in the steam dome are less than 0.1. Assuming harmonic time dependence, the wave equation reduces to the Helmholtz equation:

$$\nabla^2 P + \frac{\omega^2}{a^2} P = 0$$

where P is pressure, ω is frequency, and a is acoustic speed. The complex three-dimensional geometry of the steam dome is rendered onto a uniformly-spaced rectangular grid with mesh spacing of three inches. The solution for the pressure P is obtained for each grid point within the steam dome.

The Helmholtz equation is solved for incremental frequencies from 0 to 200 Hz, subject to the boundary conditions:

$$\frac{dP}{dn} = 0$$

normal to all solid surfaces (i.e., the steam dome wall and interior and exterior surfaces of the dryer), and:

Test canonical problems have recovered exact solutions. A representative solution at 50 Hz is shown on Figure 4-2.

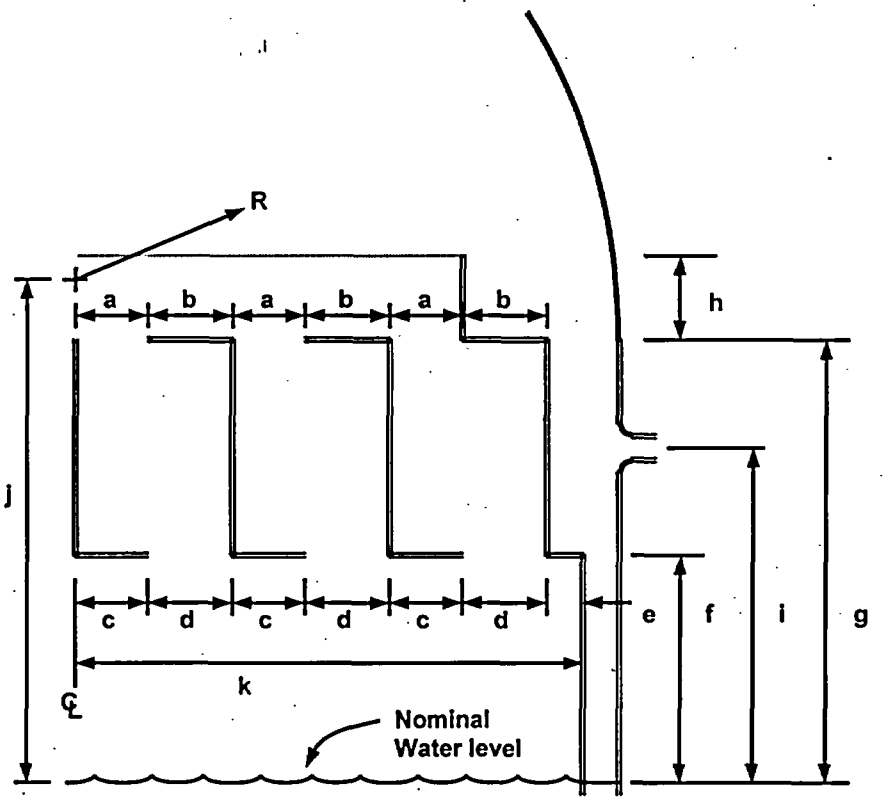

Figure 4-1 **Cross-sectional description of the steam dome and dryer, with the verified QC2 dimensions of a = 6.0 in, b = 28.5 in, c = 15.5 in, d = 19.0 in, e = 16.25 in, f = 75.0 in, g = 137.0 in, h = 23.0 in, i = 88.5 in, j = 166.63 in, k = 120.0 in, and R = 125.5 in.**

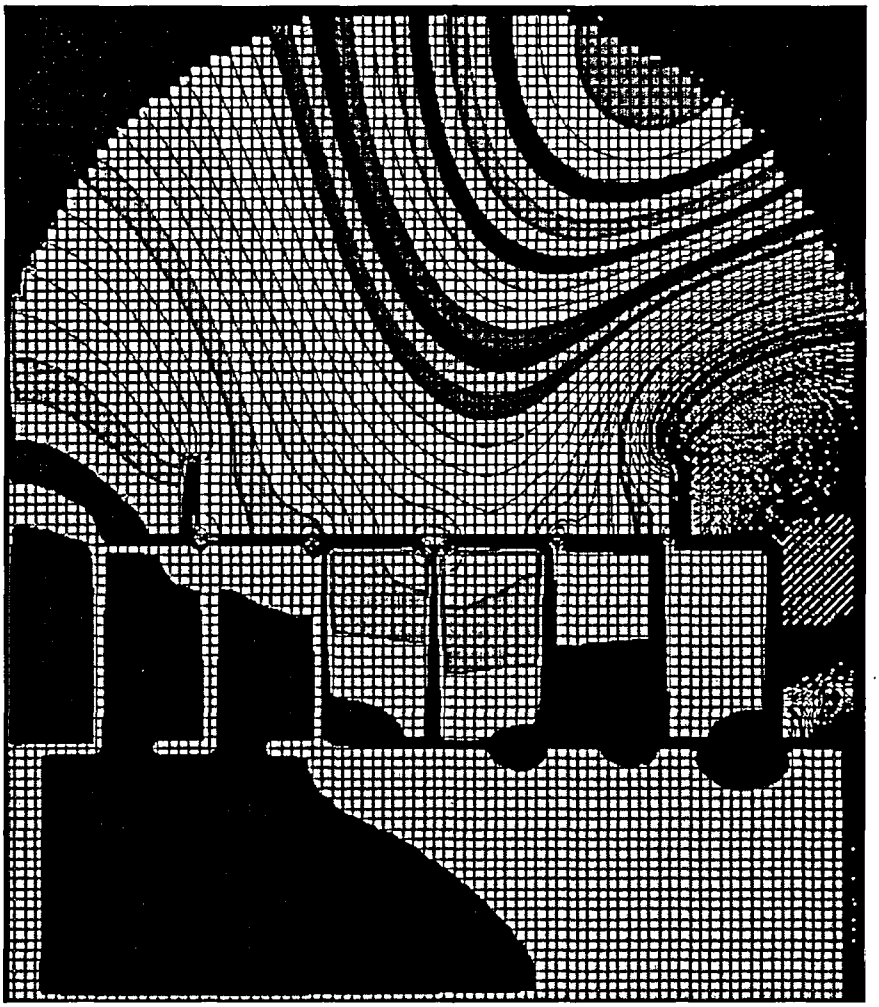

Figure 4-2 **Cross-sectional solution (180 degree azimuth) of the Helmholtz equation at 50 Hz. The right side of the figure is the midpoint between the A and B main steam vent lines, while the left side is the midpoint between the C and D main vent lines. Unit forcing is applied on the A main vent. Portions of the steam dryer are only seen in outline.**

4.2 Main Steam Lines

The Helmholtz solution within the steam dome is coupled to an acoustic circuit solution in the main steam lines. Pressure fluctuations in single-phase compressible medium, where acoustic wavelengths are long compared to characteristic length scales for the internal components and to transverse dimensions (i.e., directions perpendicular to the primary flow directions), can be determined through application of the acoustic

circuit methodology. By restricting the analysis to frequencies below 200 Hz, acoustic wavelengths are approximately 8 feet in length, which are sufficiently long compared to most components of interest such as branch junctions, etc.

Acoustic circuit analysis separates the main steam lines into elements that are characterized by length L, cross-sectional area A, mean fluid density $\overline{\rho}$, mean flow velocity $\overline{U}$, and mean fluid acoustic speed $\overline{a}$, as illustrated in Figure 4-3. Application of acoustic circuit methodology provides solutions for the fluctuating pressure P_n' and velocity u_n' for the nth element of the form:

$$P_n' = \left[A_n e^{ik_{1n}X_n} + B_n e^{ik_{2n}X_n}\right] e^{i\omega t}$$

$$u_n' = -\frac{1}{\overline{\rho a}^2}\left[\frac{\left(\omega + \overline{U}_n k_{1n}\right)}{k_{1n}} A_n e^{ik_{1n}X_n} + \frac{\left(\omega + \overline{U}_n k_{2n}\right)}{k_{2n}} B_n e^{ik_{2n}X_n}\right] e^{i\omega t}$$

where harmonic time dependence of the form $e^{i\omega t}$ has been assumed. The wave numbers k_{1n} and k_{2n} are the two complex roots of the equation:

$$k_n^2 + if_n \frac{\left|\overline{U}_n\right|}{D_n \overline{a}^2}\left(\omega + \overline{U}_n k_n\right) - \frac{1}{\overline{a}^2}\left(\omega + \overline{U}_n k_n\right)^2 = 0$$

where f_n is the pipe friction factor for the nth element, D_n is the hydraulic diameter for the nth element, and $i = \sqrt{-1}$. The complex constants A_n and B_n in the expressions for the fluctuating pressure and velocity above are a function of frequency. These constants are determined by satisfying continuity of pressure and mass conservation at the element junctions.

A similar acoustic circuit analysis is used in the instrument lines to transfer the pressure recorded at the transducer to the main steam line. This analysis is summarized in the Appendix.

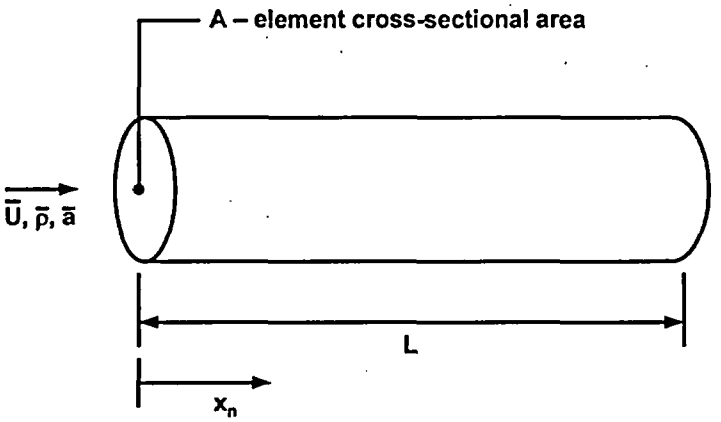

Figure 4-3 **Schematic of an element in the acoustic circuit analysis, with length L and cross-sectional area A.**

4.3 Steam Dome/Main Steam Line Junction

4.4 Branch Line Junction

4.5 Control Valves

Control valves are located before the inlets to the steam turbine and represent the end of the modeled system. Control valves, which are typically open 40%, are modeled with the assumption that downstream acoustic disturbances do not propagate upstream through the valve. This assumption is approximate and becomes more valid as the pressure drop across the valve is increased.

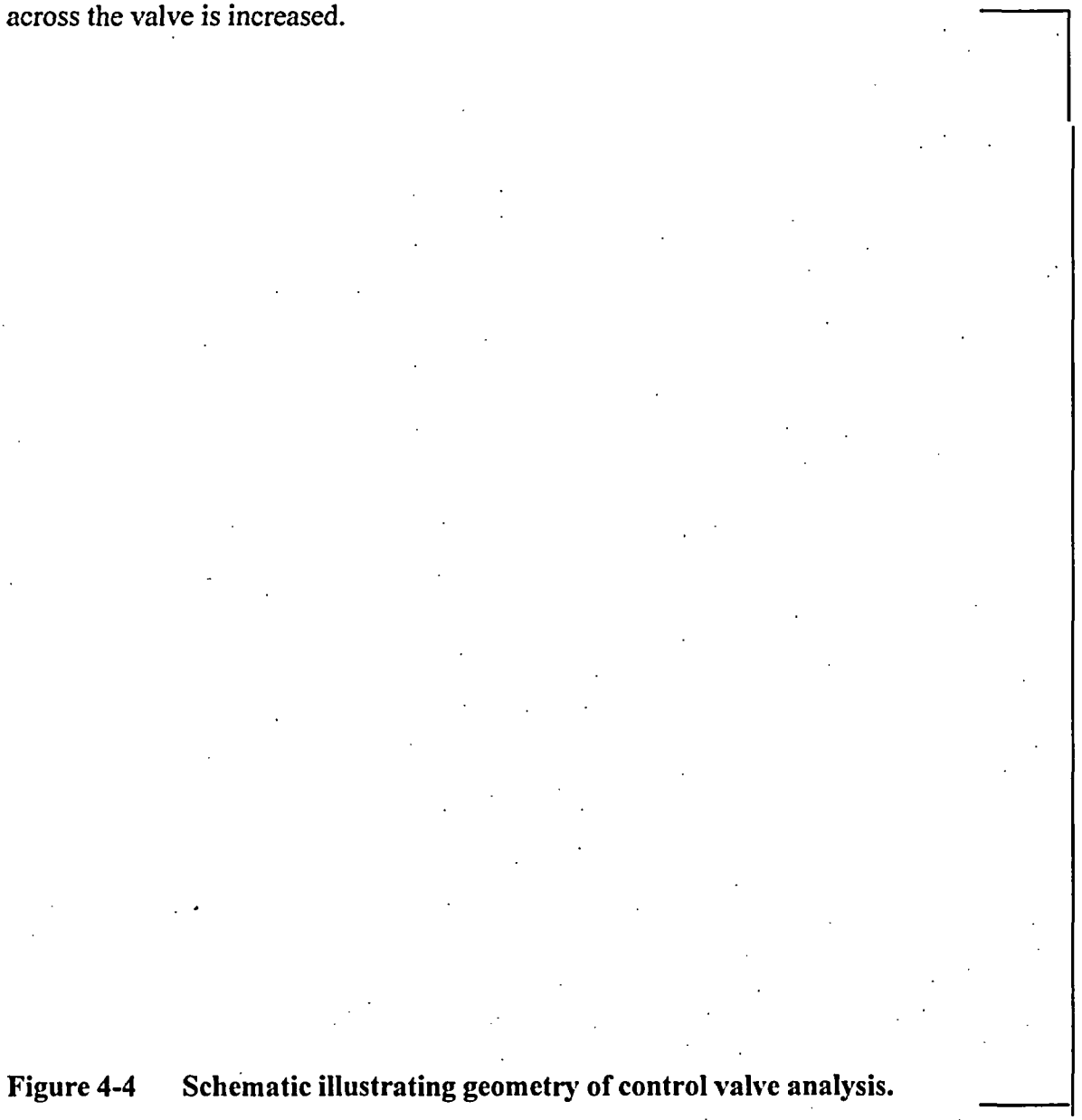

Figure 4-4 Schematic illustrating geometry of control valve analysis.

5. Model Assembly

The assembly of the loads transfer methodology is illustrated below in Figure 5-1.

Figure 5-1 Schematic of the assembled model for a D-ring plant showing source locations and locations of measured data.

In-plant data have been obtained as a function of power level. At a given power level, pressure time histories are available at the following locations:

N11A(t) - at the reactor wall at 45° azimuth

N11B(t) - at the reactor wall at 225° azimuth

VA(t) - on the main steam line at venturi A

VB(t) - on the main steam line at venturi B

VC(t) - on the main steam line at venturi C

VD(t) - on the main steam line at venturi D

TA(t) - on the main steam line at turbine instrument line A

TB(t) - on the main steam line at turbine instrument line B

TC(t) - on the main steam line at turbine instrument line C

TD(t) - on the main steam line at turbine instrument line D

SB(t) - hoop stress converted to steam line pressure upstream of the line B ERVs

In total, eleven independent data sets are available. The model in Figure 5-1 has twelve unknown sources, which are:

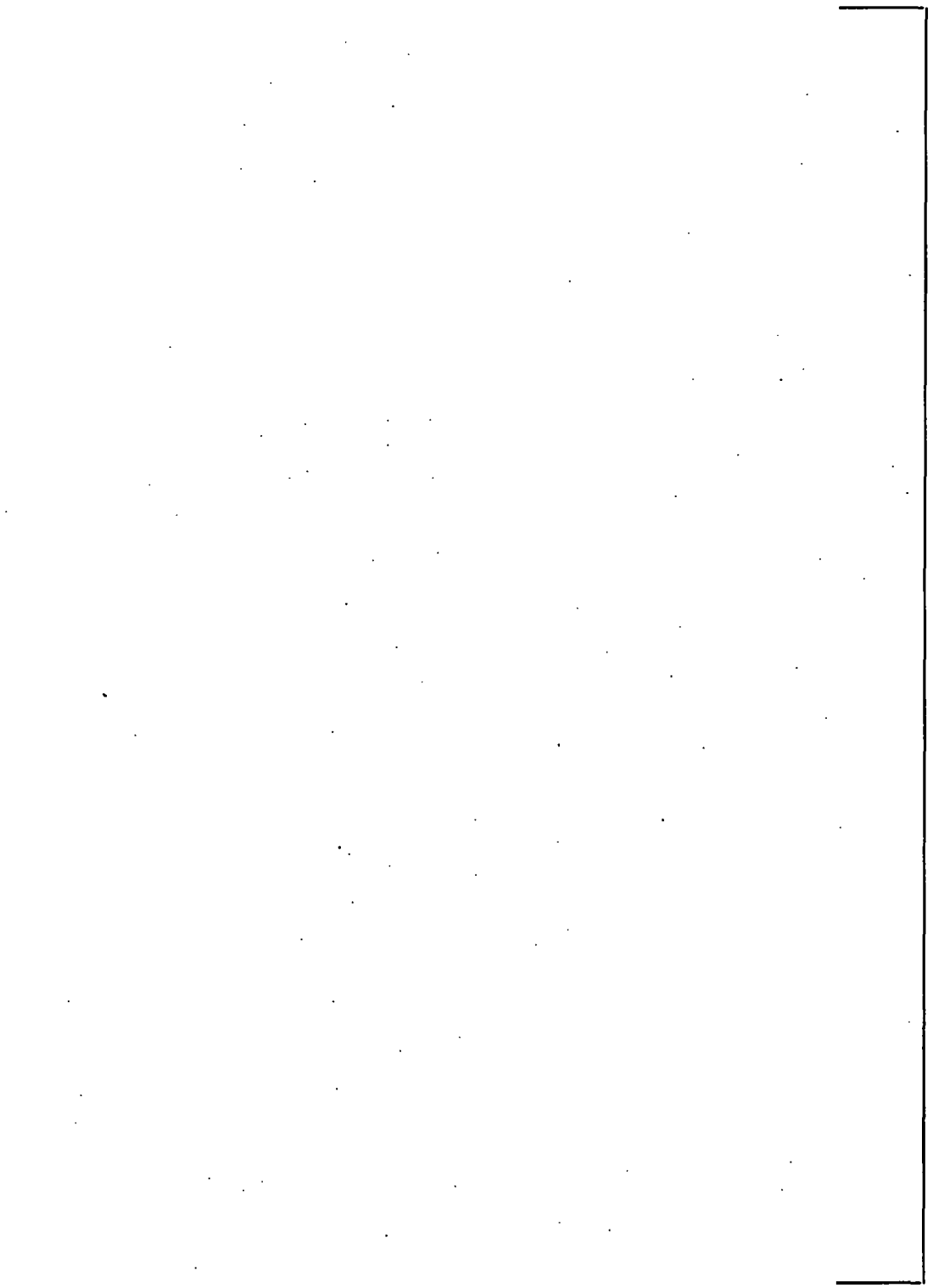

Figure 5-2 Idealization of flow field entering steam lines.

6. EPU Loads for Quad Cities Unit 2 (Example Calculation)

This section summarizes results from example calculations using the loads transfer methodology. The example uses measured data from the Quad Cities Unit 2 (QC2) steam supply system during extended power uprate (EPU) operation.

6.1 Dryer Peak Pressures

Calculations have been performed using measured EPU data

Peak pressures and root mean square (RMS) pressure levels are predicted at different dryer locations (node numbers) in Figure 6-1. Physical node locations are shown in Figure 6-2.

6.2 Dryer Time History

The differential pressure and associated power spectral density (PSD) across the cover plate is shown in Figure 6-3. In principle, the model can predict the pressure time history at any location in the steam dome to a resolution of approximately three inches. Examination of the pressure spectrum (PSD) indicates that energy exists at discrete frequencies in the pressure time history.

6.3 Validation

As discussed previously, the strain gauge data SB(t) on the B line upstream of the ERVs has not been used in the analysis to provide a separate dataset for model validation. The estimated pressure in the main steam line from strain gage data is shown in Figure

6-4 with its associated PSD. Several calculations were performed varying the bulk acoustic speeds in the instrument lines, and the results of these calculations are shown in Figure 6-5 and Figure 6-6, providing predictions of the pressure at this location for bulk instrument line acoustic speeds of 4600 ft/sec and 4700 ft/sec, respectively. Referring to Figure 6-7 below, these acoustic speeds correspond to bulk instrument line water temperatures of 348.3°F and 326.1°F, respectively.

A comparison of data from Figure 6-4 with model predictions is tabulated below. Comparison of the PSDs shows similar frequency content between measured and predicted pressures.

	Peak Pressure (psid)	P_{rms} (psid)
SB	11.44	2.80
Prediction 4600 ft/sec	11.41	2.80
Prediction 4700 ft/sec	11.82	2.79

6.4 Model Uncertainty

The loads transfer methodology to determine the pressure fluctuation magnitudes on the reactor walls or in the main steam lines is undergoing additional validation using a separate full-scale test program. Once this validation program is complete, the measured pressure data will be subject to uncertainty associated with instrumentation measurement accuracy and the assumed acoustic speed in the instrument lines.

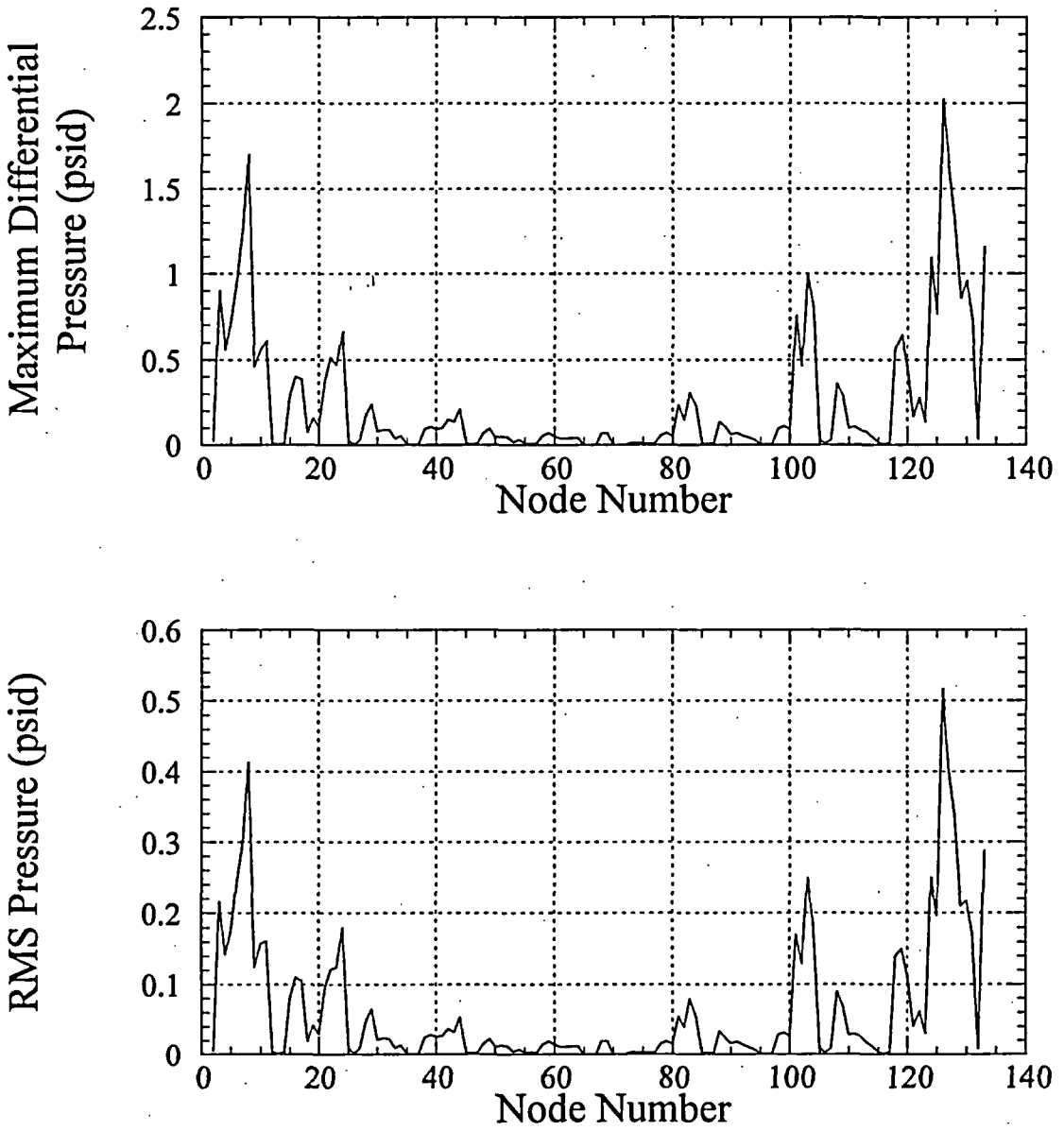

Figure 6-1 EPU loads developed by the current methodology.

TOP VIEW:

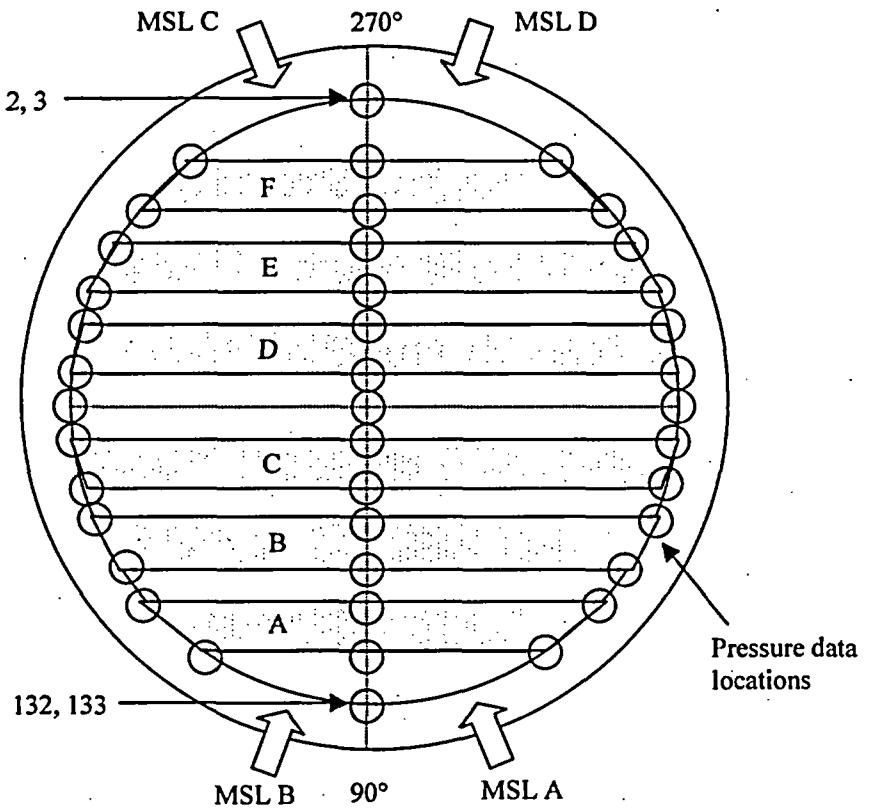

SIDE VIEW:

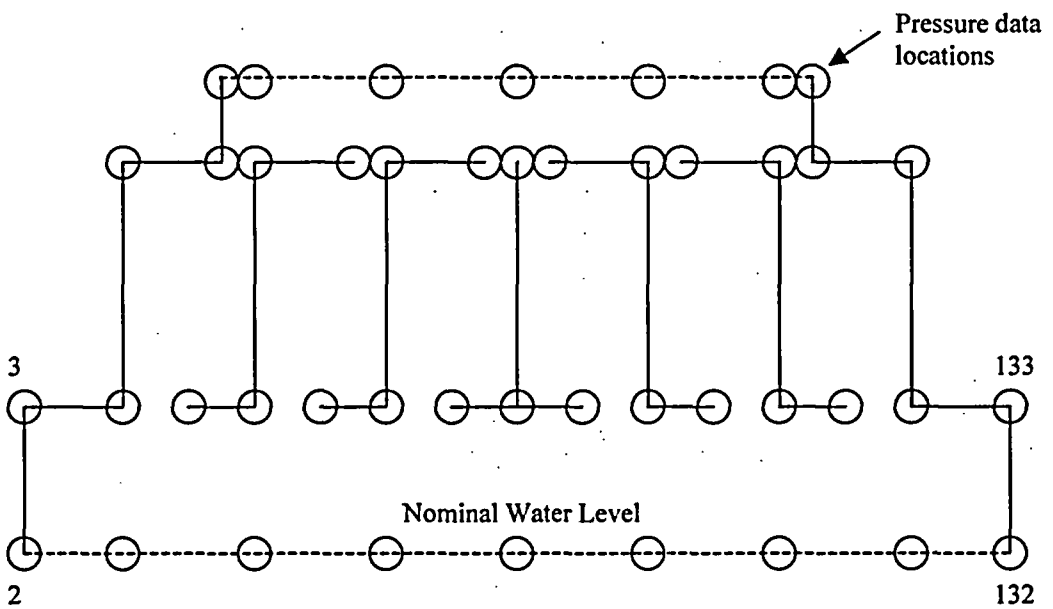

Figure 6-2 Top and side view schematic of pressure node locations on the steam dryer.

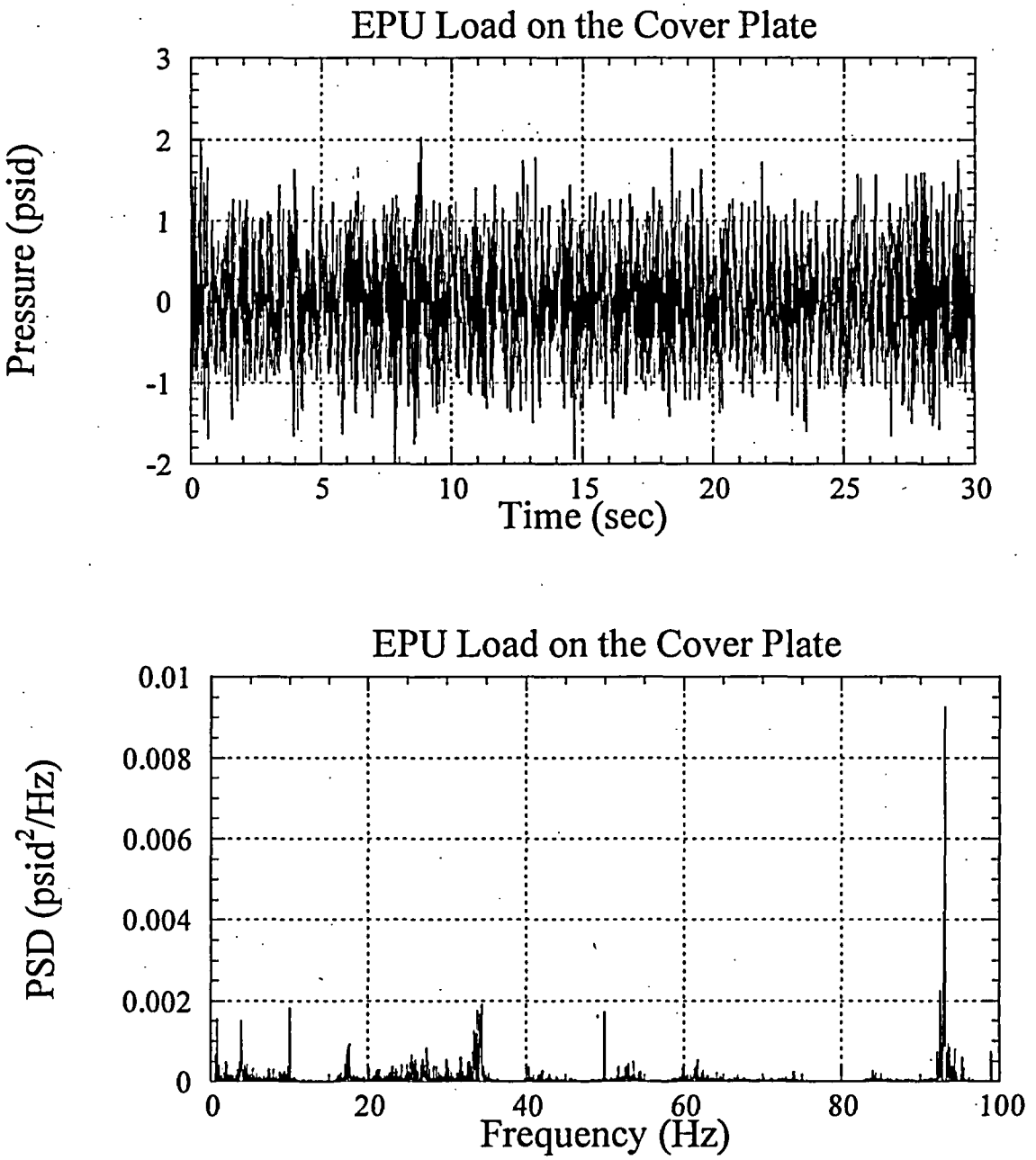

Figure 6-3 **EPU pressure time history and PSD on the cover plate on the A and B main vent side.**

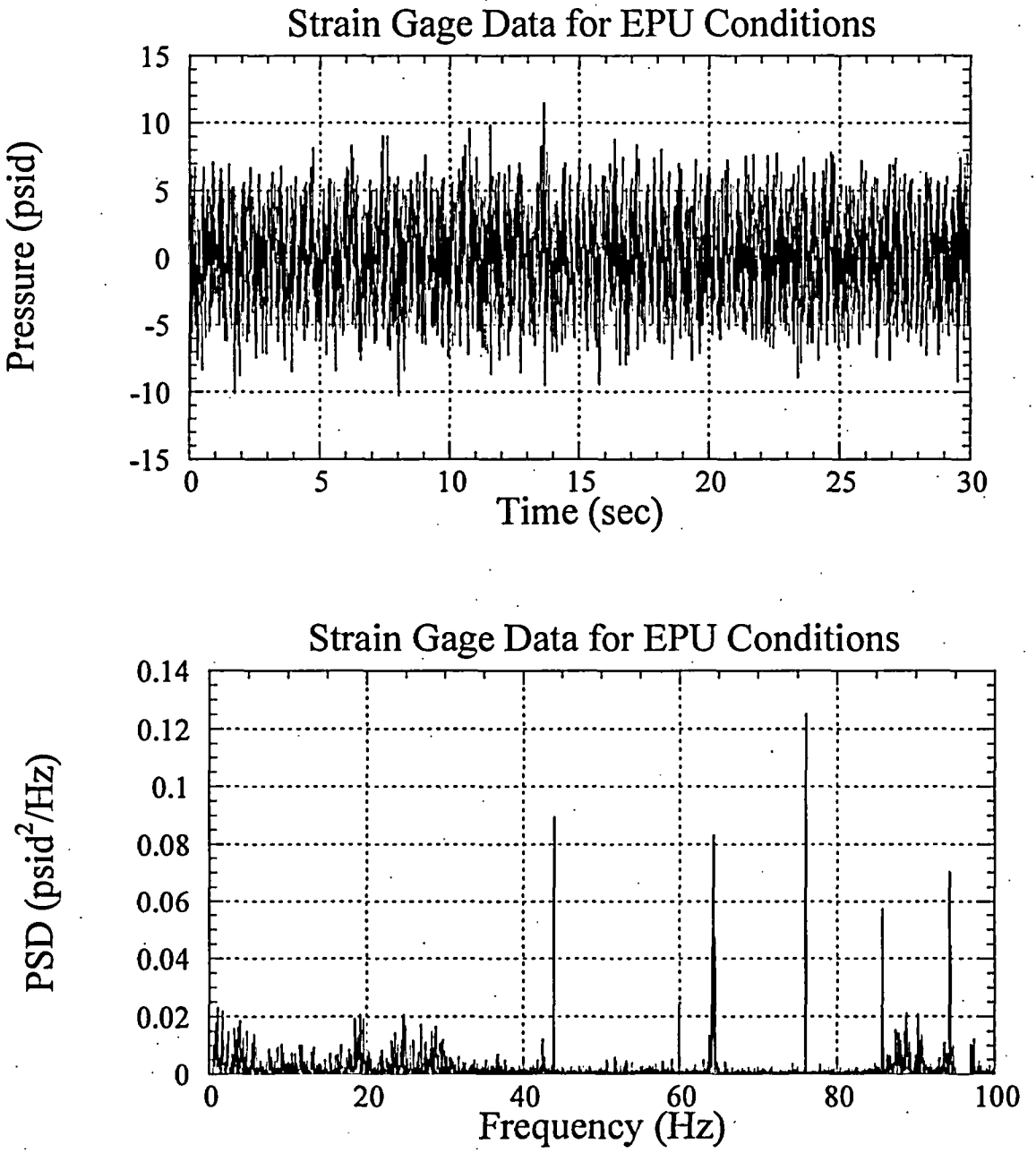

Figure 6-4 EPU pressure time history and PSD derived from strain gage data.

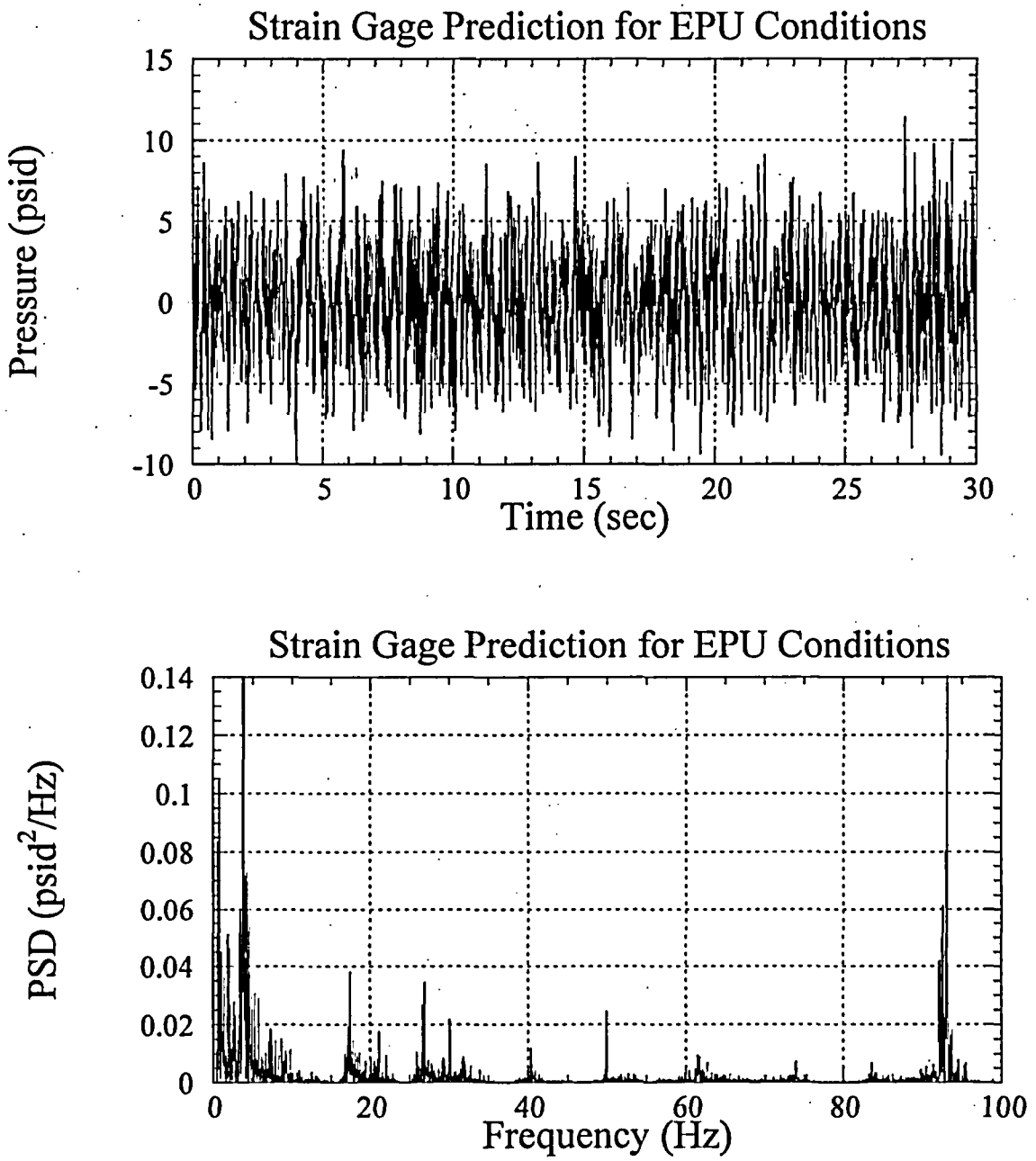

Figure 6-5 EPU strain gage pressure and PSD predictions with the current methodology, for an acoustic speed of 4600 ft/sec.

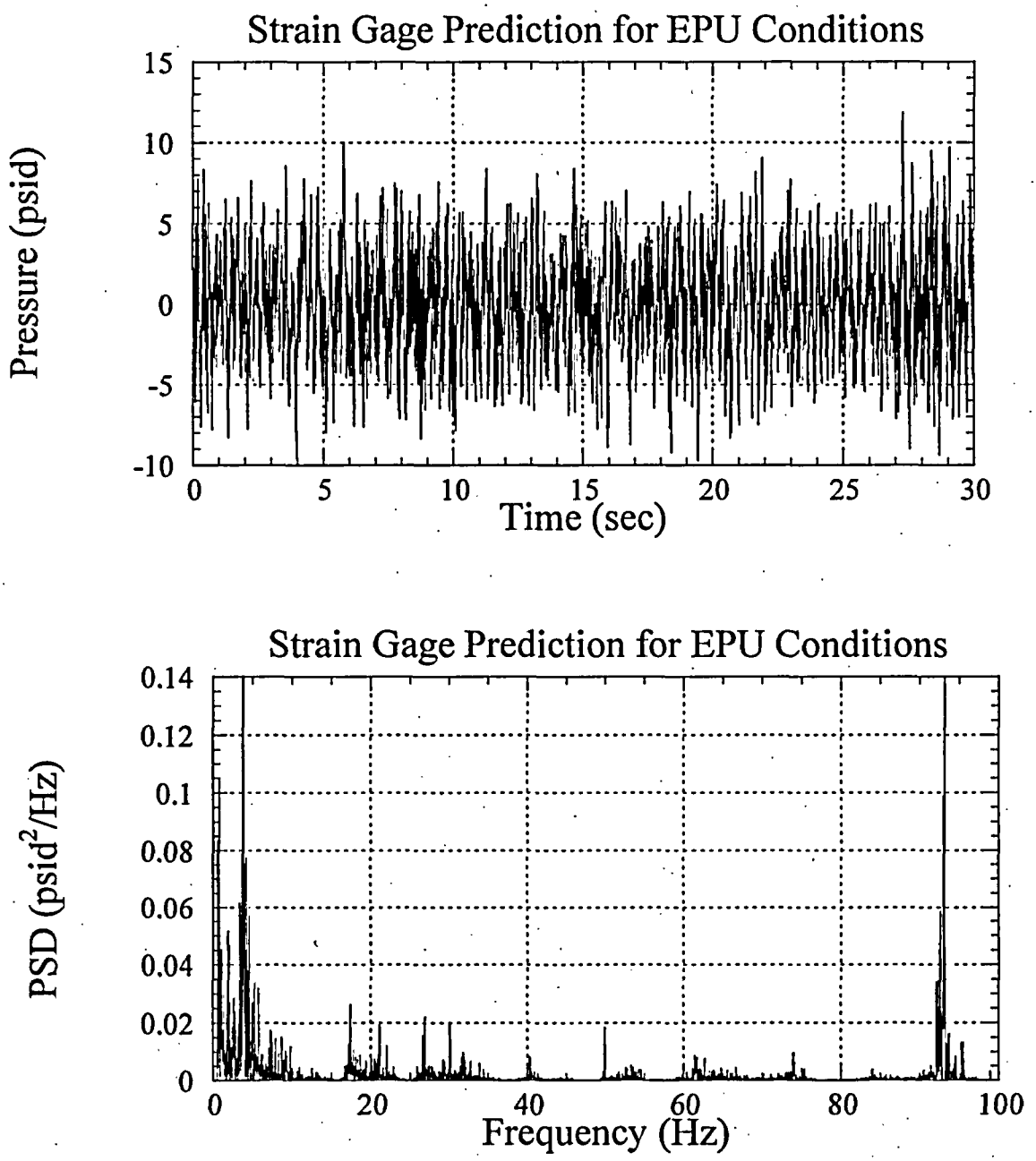

Figure 6-6 **EPU strain gage pressure and PSD predictions with the current methodology, for an acoustic speed of 4700 ft/sec.**

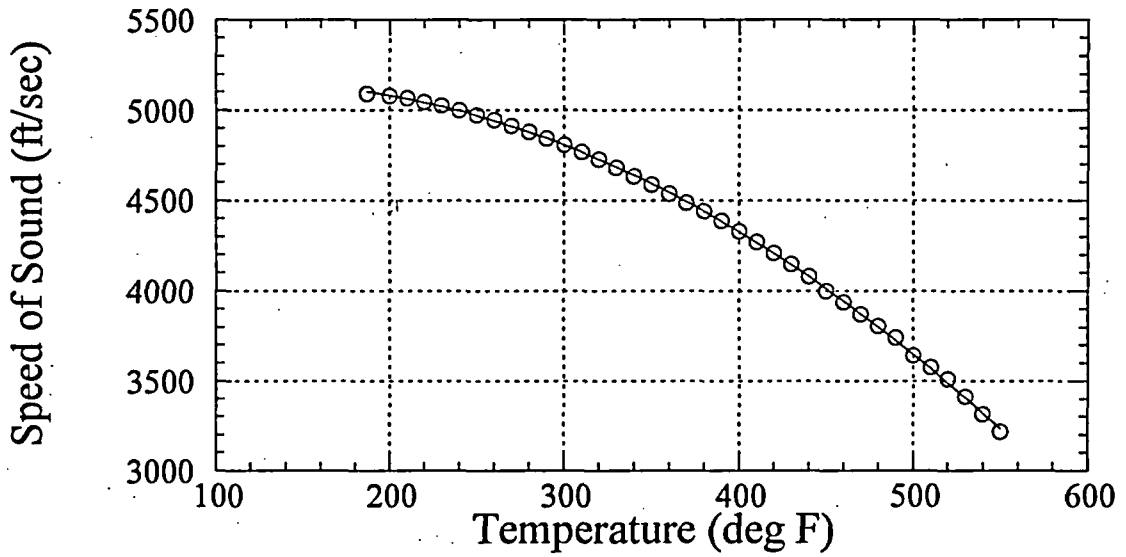

Figure 6-7 Temperature effect on water acoustic speed [7].

7. Sensitivity Analysis

The sensitivity of the peak loads on the dryer to the acoustic speed can be determined from the computed dryer loads at two bulk instrument line acoustic speeds. This sensitivity ($\partial P/\partial a$) is shown in Figure 7-1 at an instrument line bulk acoustic speed of 4700 ft/sec. For the predicted load to have an accuracy of 10%, the bulk acoustic speed must be known to within 500 ft/sec.

The sensitivity to instrument measurement error can also be evaluated. This evaluation is required since the pressure fluctuations measured on the reference leg transducers are near the resolution limits of at least one transducer. Calculations were run by increasing the water level transducers by 20%. The changes in the predicted peak pressures on the dryer are shown in Figure 7-2. It is apparent that the dryer load definition uncertainty benefits from water level measurements with improved accuracy.

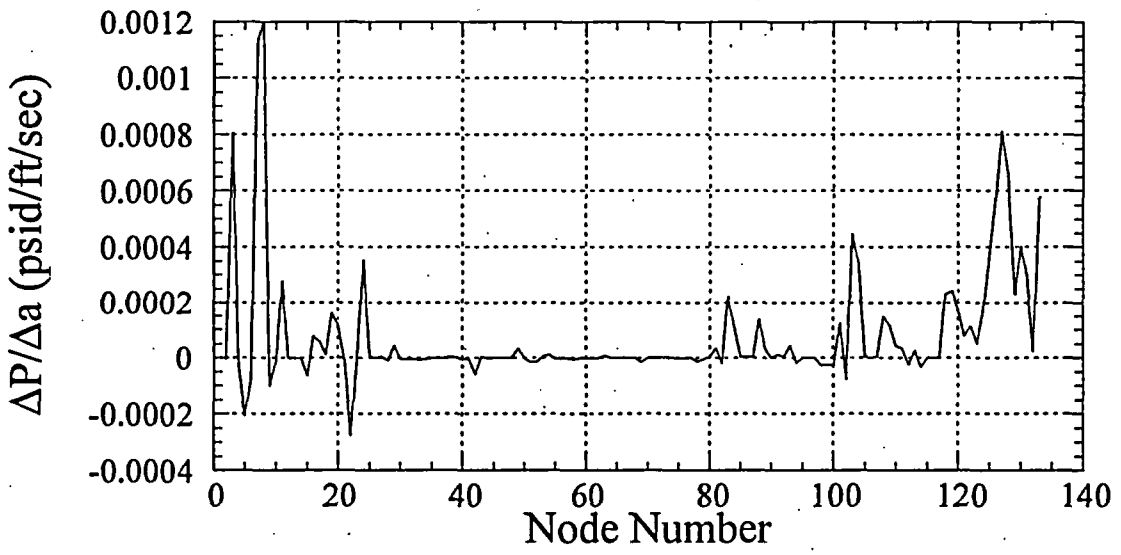

Figure 7-1 Sensitivity of the dryer loads to change in acoustic speed.

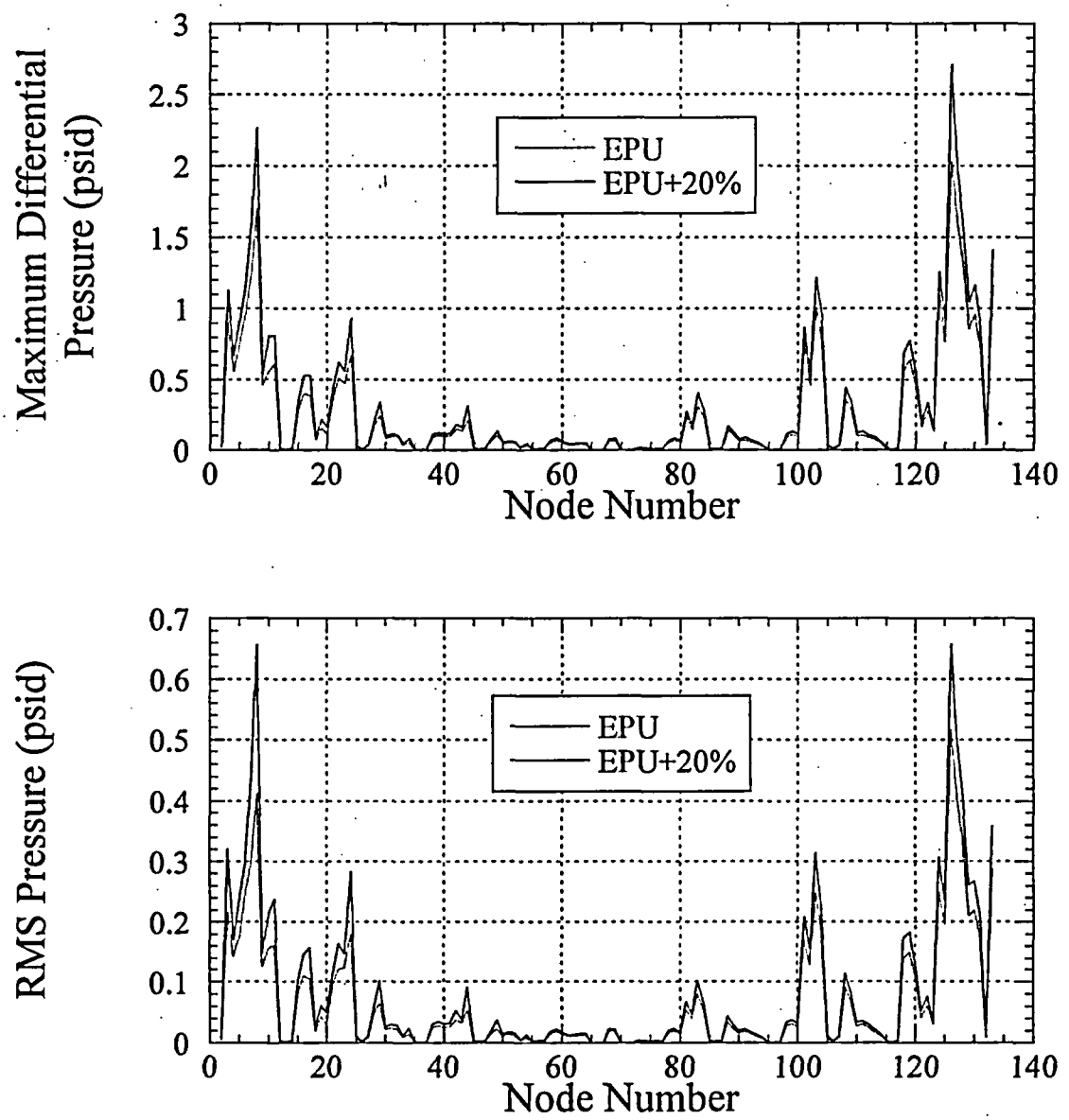

Figure 7-2 **EPU loads developed by the current methodology, with a 20% increase in EPU loads for an acoustic speed of 4700 ft/sec.**

8. Conclusions

A physically-based, loads transfer methodology that can predict loads on reactor components from measurements made external to the reactor steam dome has been developed and validated. The model accounts for acoustic sources at locations along the steam delivery system that are known to provide a region where mean flow energy can be transferred in acoustic pressure oscillations. Accuracy of the model-based loads transfer scheme is most likely limited by in-plant pressure measurement accuracy, and these errors are therefore quantifiable. Following validation of instrument correction algorithms, not discussed in this report, the methodology should reliably provide definition of plant-unique dryer loads.

9. References

1. Continuum Dynamics, Inc., "Hydrodynamic Loads on Quad Cities Unit 1 Steam Dryer," CDI Report No. 03-18, 2003.
2. Continuum Dynamics, Inc., "Hydrodynamic Loads on Dresden Unit 2 Steam Dryer," CDI Report No. 04-01, 2004.
3. Continuum Dynamics, Inc., "Hydrodynamic Loads on Dresden Unit 3 Steam Dryer," CDI Report No. 04-02, 2004.
4. Weaver, D.S. and MacLeod, G.O., "Entrance Port Rounding Effects on Acoustic Resonance in Safety Relief Valves," PVP-Vol. 389, Flow-Induced Vibration, 1999 ASME Pressure Vessels and Piping Conference, Boston, MA, August 1999.
5. Ziada, S., "A Flow Visualization Study of Flow-Acoustic Coupling at the Mouth of a Resonant Side-Branch," PVP Vol. 258, Flow-Induced Vibration and Fluid Structure Interaction, 1993 Pressure Vessels and Piping Conference, Denver, CO, July 1993.
6. Tu, T., "Verification of Dimensions for Quad Cities 1 & 2 and Dresden 2 & 3 Steam Dome and Steam Dryer," GE-NE-0000-0026-6917-11, Rev. 1, 2004.
7. McDade, J. C., D. R. Pardue, A. L. Hedrich and F. Vrataric, "Sound Velocity in Water above 212°F," The Journal of the Acoustical Society of America, 31(10): 1380-1383, 1959.

10. Appendix

ATTACHMENT 5

Exelon Report No. AM-2004-006

CDI Benchmark Results of GE Scale Model Test Facility

AM-2004-006

CDI Benchmark Results of GE Scale Model Test Facility

Prepared By K. B. Rund Date 12/1/04

Reviewed By Keith Moser Date 12/1/04

CDI Benchmark Results of GE Scale Model Test Facility

12/1/2004

Background

Continuum Dynamics (CDI) developed an acoustic circuit (AC) analysis of the steam lines and a three dimensional acoustic model of the vessel steam space to help define Dresden and Quad Cities dryer loads. The original acoustic circuit model was based on the current Quad Cities dryer dimensions and test data gathered from QC2 and verification was limited to the instrument line mockup performed at the CDI facility. A benchmark was developed to validate the CDI model using results from the GE scale model facility testing. This paper was generated to document the validation results and to identify any inconsistencies between the acoustic circuit and the GE scale model test (SMT).

Benchmark Approach

To perform the benchmark, GE provided scale model test as-built dimensions to CDI and CDI provided GE with the acceptable scale model steam path microphone locations. CDI was then provided with measured data from transducers on the GE scale model steam line to acoustically predict the pressure fluctuation response of transducers placed inside the scale model test vessel. The scale model test parameters are as follows:

Physical scale of the model	1 to 17.3
Frequency Scale of QC1 actual to SMT	1 to 12.13
Pressure Scale of QC1 to SMT	65 to 1
Q_{OLTP} As Scaled	165 CFM
Q_{EPU} As Scaled	197 CFM
Sampling Rate	8192 Hz
Blind Sample Points	M9 and M21
Flow rate for the Benchmark Test Data Between 70 and 73 Seconds	270 CFM

Data from two microphones was withheld as a blind sample to compare the predicted values from the acoustic model to the actual values from the scale model microphones. The locations of the two microphone withheld (M9 and M21) are shown on Figure 1. Microphones 9 and 21 are located at the same spot on the vertical hood on opposite ends (90 and 270 degrees) of the dryer.

CDI performed the benchmark twice. The first benchmark showed reasonable results but it was identified that the annulus between the dryer skirt and the vessel wall had been modeled as an air gap open to the volume below it. This configuration does not correlate to the SMT, which has this annulus sealed off. To explore the sensitivity of the results to this modeling assumption, CDI performed a second benchmark case, which closed the lower annulus boundary. The CDI analyses were performed to ensure converged solutions were obtained to a minimum of 2426 Hertz subscale test frequency, corresponding to 200 hertz for the actual plant data.

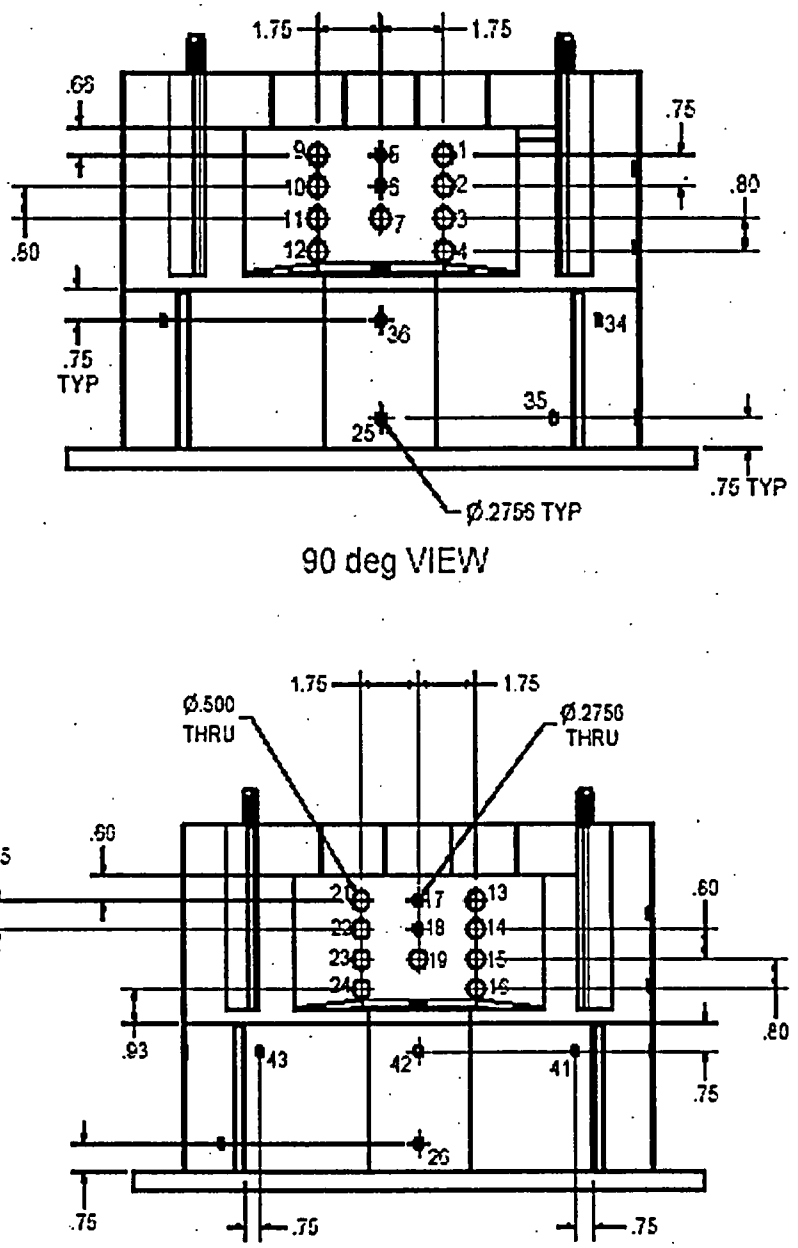

Figure 1 – Microphone Locations on Dryer Model
Microphone location 9 in top drawing (90 degree view)
Microphone location 21 in bottom drawing (270 degree view)

Benchmark Data/Results

The original data provided to Exelon by CDI contained data that did not converge above 2426 hertz due to time constraints in running the acoustic model. Therefore, a Fast Fourier filtering process was applied to both the test data and the CDI predicted data to ensure appropriate comparisons could be made. This allowed a comparison based only on the converged solutions.

In addition, Fast Fourier Transforms (FFT) of the measured data was performed for each of the benchmarks to confirm the pressure loads above 2426 hertz were insignificant. The raw data results for both benchmark tests at each blind test location are shown in Appendix A.

Power Spectral Density (PSD) plots were computed for the filtered test data as well as each computed point and are provided in Appendix B. These allow additional checks of frequency dependent behavior and identify any random vibration. The typical units used in the PSD plots are acceleration (amplitude is the square of the root-mean-square divided by frequency (RMS^2/Hz)) on the vertical scale and frequency (Hz) on the horizontal scale.

A comparison of the filtered SMT and CDI predicted data for the two benchmark tests at each blind test location and data results are provided below.

Comparison of Results for Data Point M9:

First Benchmark (No Annular Seal in CDI Model) – Data Point M9:

Raw Data M9	CDI Predicted Data M9
mean(zf) = 0	mean(zfl) = 0
Stdev(zf) = 17.31453	Stdev(zfl) = 19.88286
max(zf) = 59.64194	max(zfl) = 67.62408
min(zf) = –64.09427	min(zfl) = –80.88236

Plot of Filter SMT data (Red) compared to CDI predicted data (Blue) -
First Benchmark Data Point M9

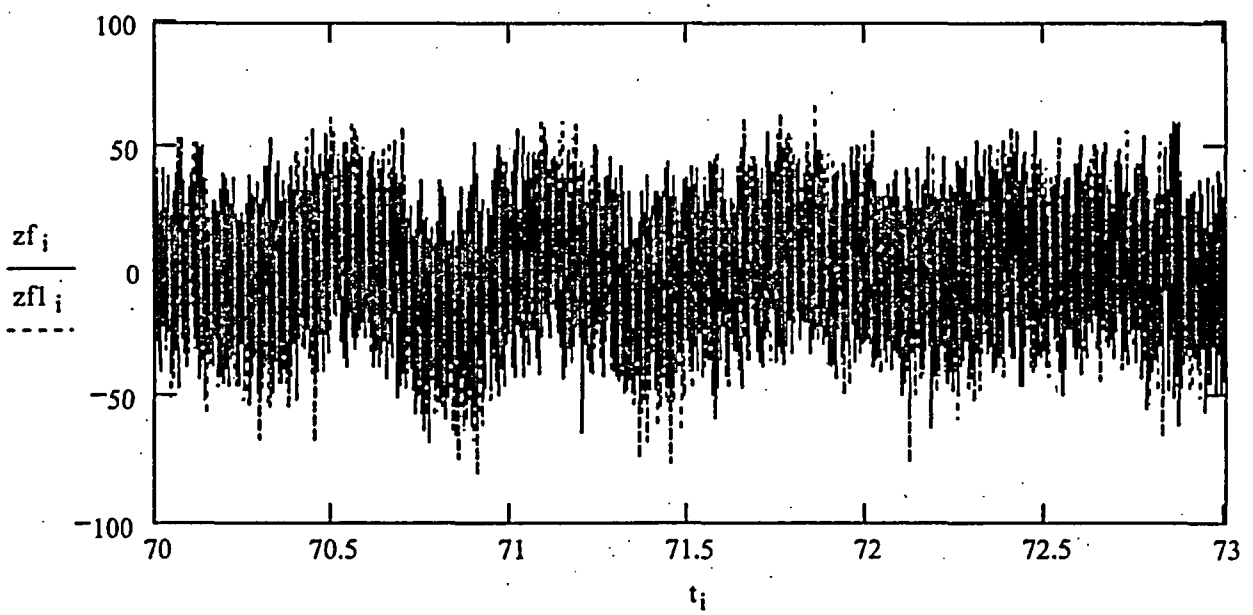

Figure 2 - First Benchmark – M9
Comparison in the time domain
Plot of filter SMT data (red) compared to CDI predicted (blue)

Plot of Filter SMT data (Red) compared to CDI predicted data (Blue) -
First Benchmark Data Point M9

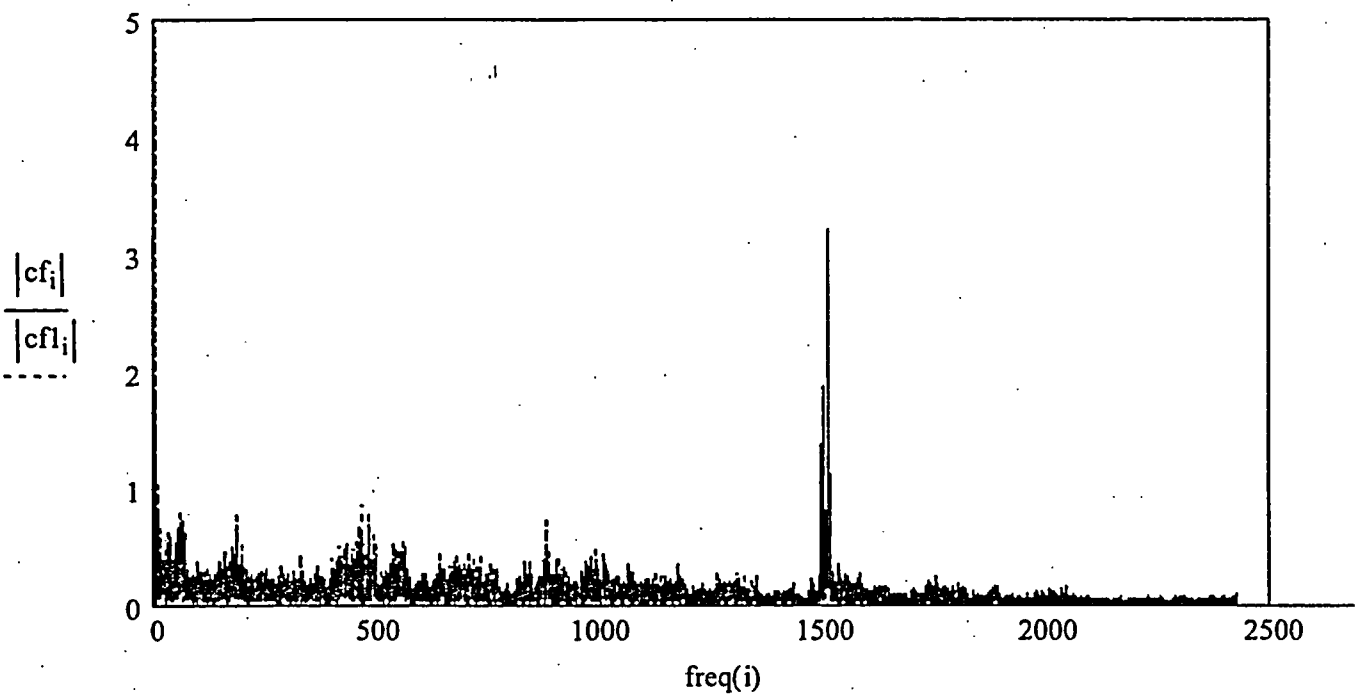

Figure 3 - First Benchmark – M9
Comparison in the frequency domain
Plot of filter SMT data (red) compared to CDI predicted (blue)

Second Benchmark (With Annular Seal in CDI Model) – Data Point M9:

SMT Filter data Point M9	CDI Predicted Data Point M9
mean(zf) = 0	mean(zfl) = -1.38005×10^{-15}
Stdev(zf) = 17.31453	Stdev(zfl) = 27.6108
max(zf) = 59.64194	max(zfl) = 108.71954
min(zf) = –64.09427	min(zfl) = –111.37362

Plot of Filter SMT data (Red) compared to CDI predicted data (Blue) - Second Benchmark Data Point M9

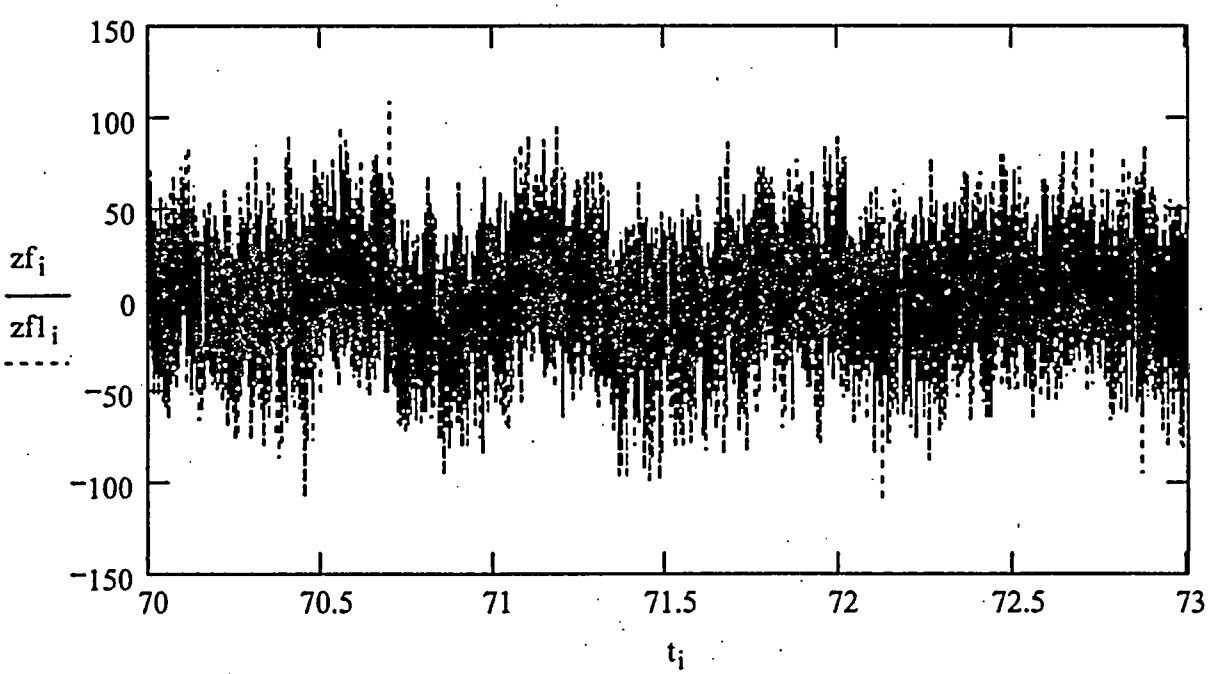

Figure 4 - Second Benchmark – M9
Comparison in the time domain
Plot of filter SMT data (red) compared to CDI predicted (blue)

Plot of Filter SMT data (Red) compared to CDI predicted data (Blue) -
Second Benchmark Data Point M9

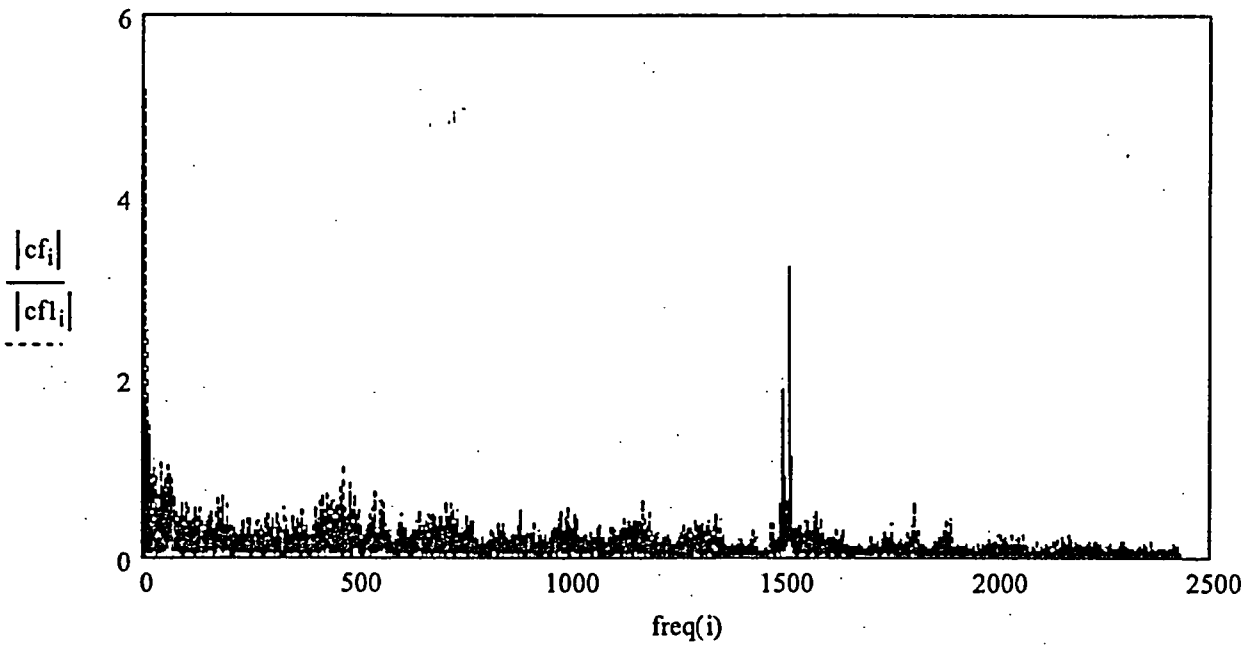

Figure 5 - Second Benchmark – M9
Comparison in the frequency domain
Plot of filter SMT data (red) compared to CDI predicted (blue)

Comparison of Results for Data Point 21:

First Benchmark (No Annular Seal in CDI Model) – Data Point M21:

Raw Data M21	CDI Predicted Data M21
mean(zf) = 3.70093×10^{-15}	mean(zfl) = 1.46813×10^{-15}
Stdev(zf) = 22.06467	Stdev(zfl) = 20.146
max(zf) = 71.23197	max(zfl) = 70.63575
min(zf) = –86.15166	min(zfl) = –81.85192

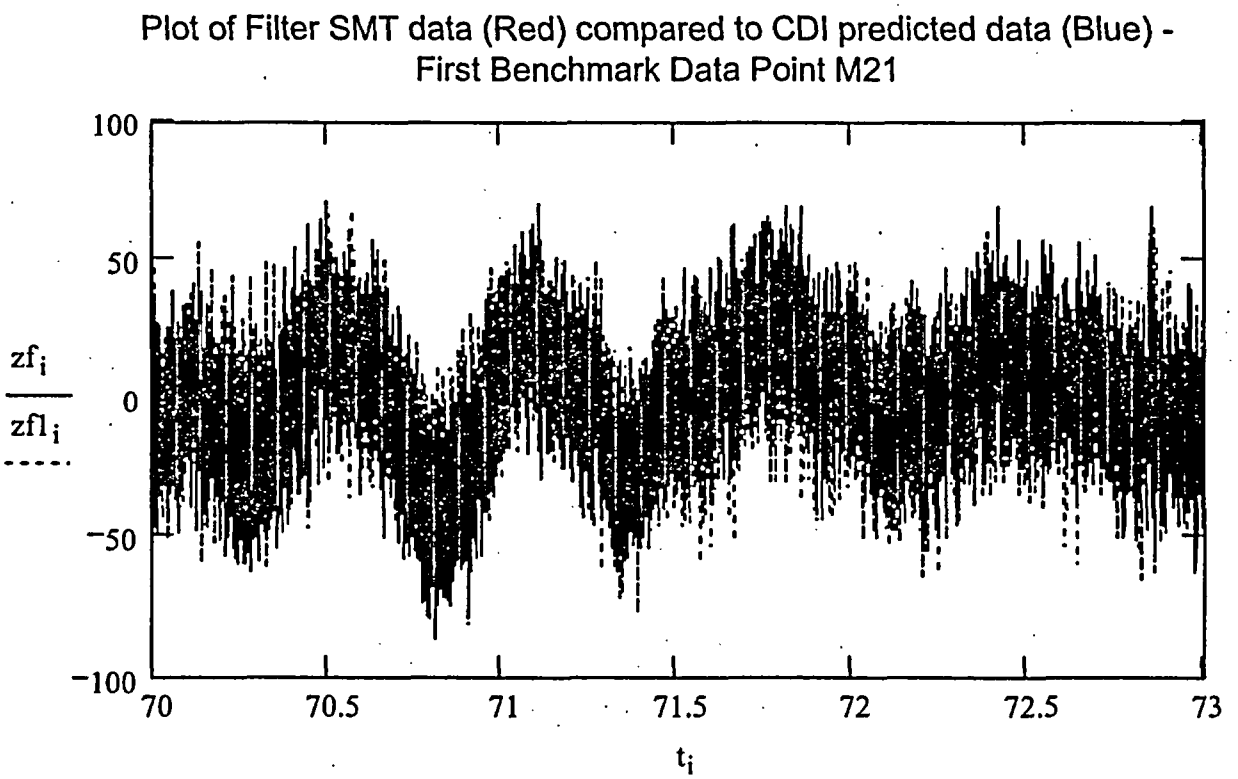

Figure 6 - First Benchmark – M21
Comparison in the time domain
Plot of filter SMT data (red) compared to CDI predicted (blue)

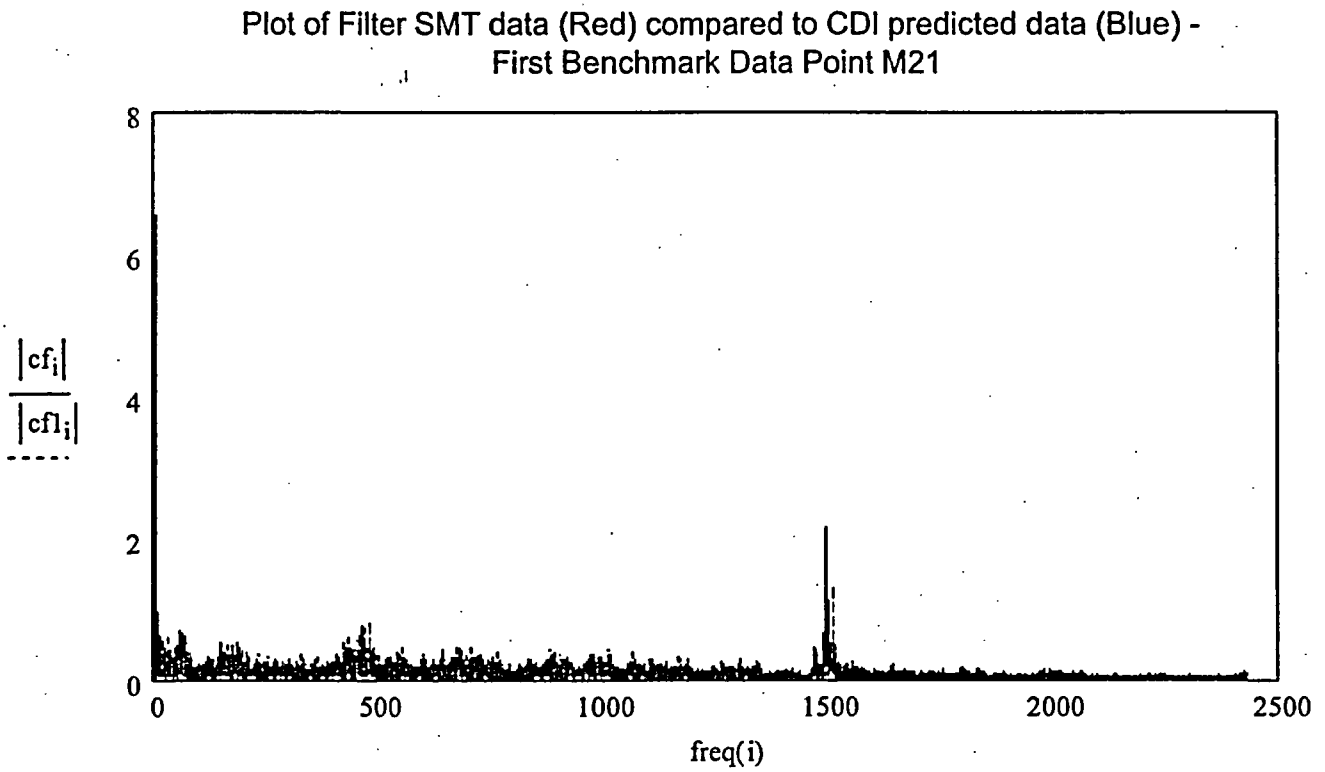

Figure 7 - First Benchmark – M21
Comparison in the frequency domain
Plot of filter SMT data (red) compared to CDI predicted data (blue)

Second Benchmark (With annular seal in CDI model) – Data Point M21:

Raw Data M21	CDI Predicted Data M21
mean(zf) = 3.70093×10^{-15}	mean(zfl) = 0
Stdev(zf) = 22.06467	Stdev(zfl) = 27.93405
max(zf) = 71.23197	max(zfl) = 102.66728
min(zf) = −86.15166	min(zfl) = −138.68934

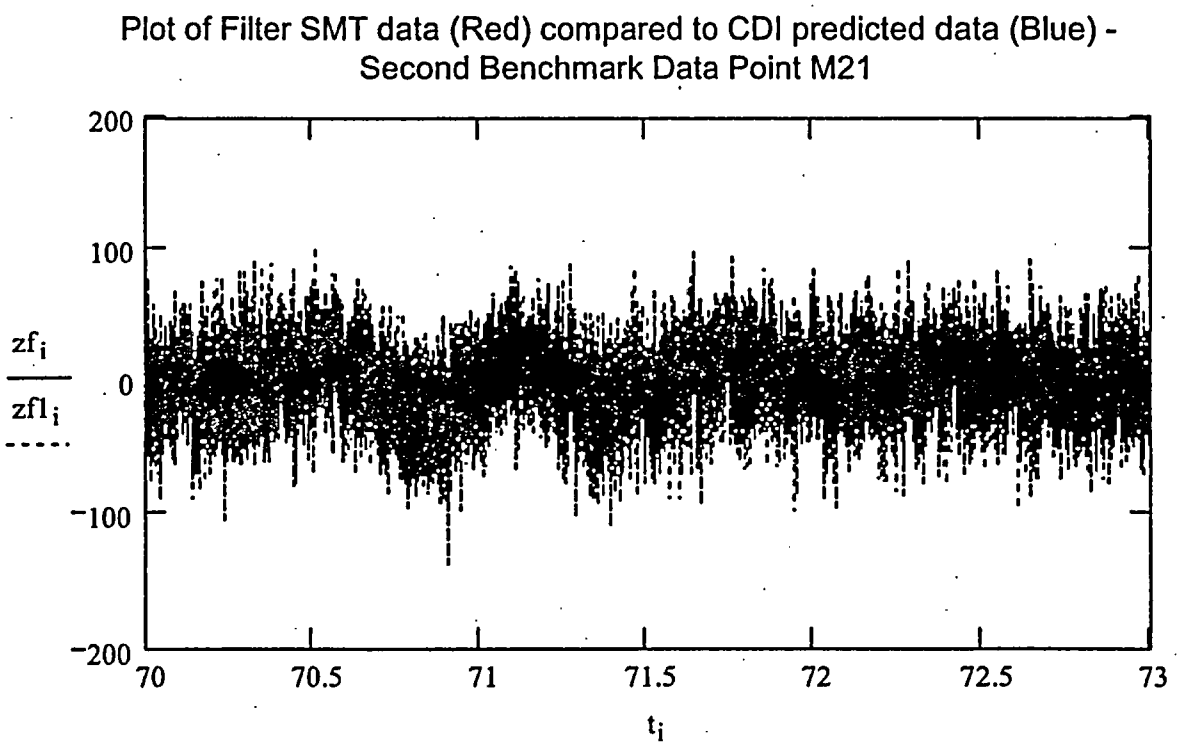

Figure 8 - Second Benchmark – M21
Comparison in the time domain
Plot of filter SMT data (red) compared to CDI predicted (blue)

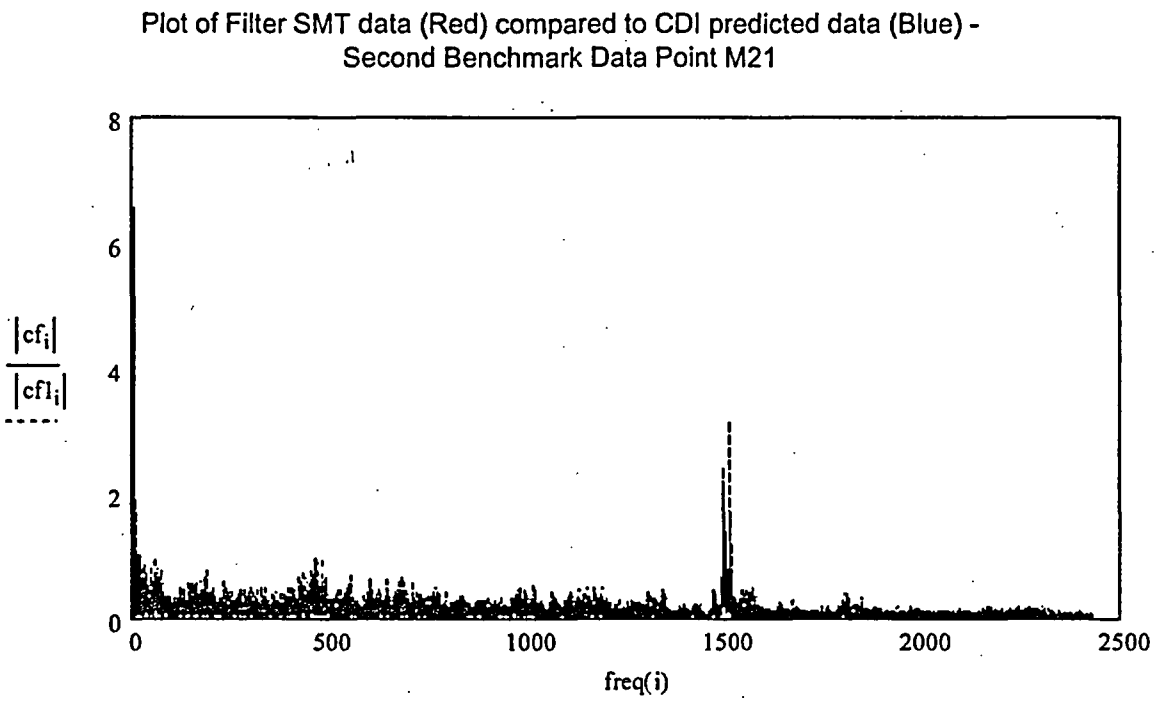

Figure 9 - Second Benchmark – M21
Comparison in the frequency domain
Plot of filter SMT data (red) compared to CDI predicted (blue)

Benchmark Conclusion

The benchmark comparisons provide a number of conclusions:

1) The CDI model shows very good fidelity to the test data, following the trends well as shown in the time history information. It is apparent from the Power Spectral Density plots that the acoustic circuit model has a strong 1500 Hz component (124 Hz scaled), which is also found in the GE scale model test results.

2) The CDI model tends to be conservative relative to the test data, but not unreasonably so.

3) The differences in results of the first and second models are relatively small. The first model appears to yield results more closely matching the test data, while the second model is more conservative.

These conclusions support the overall conclusion that CDI acoustic methodology is capable of accurately representing acoustic phenomena in the reactor vessel steam path, both in terms of the absolute pressure magnitudes as well as the spatial relationships. This test comparison provides a good benchmark of the methodology.

Appendix A

SMT Raw Data Results: Test data point M9

$\text{mean}(\text{Data}^{\langle 1 \rangle}) = -0.50679$	mean value
$\text{stdev}(\text{Data}^{\langle 1 \rangle}) = 17.52929$	standard deviation
$\max(\text{Data}^{\langle 1 \rangle}) = 64.12854$	maximum
$\min(\text{Data}^{\langle 1 \rangle}) = -66.38837$	minimum

Plot of original data M9

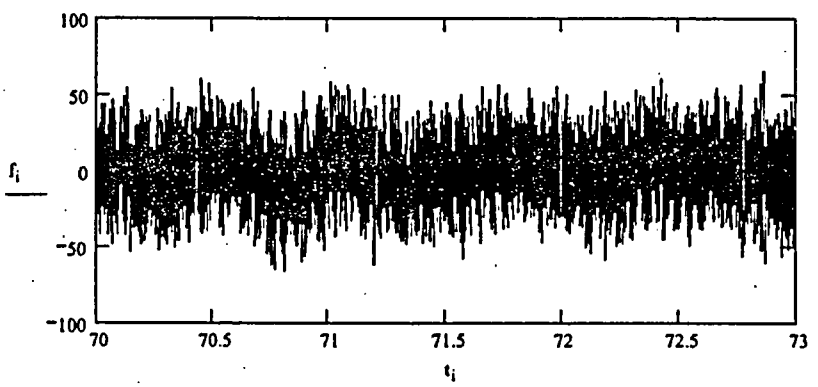

Plot of the magnitude of the fourier coefficients as a function of frequency M9

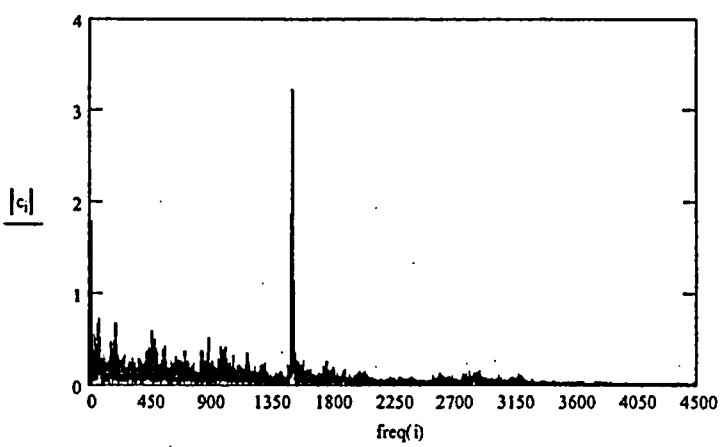

Appendix A

SMT Raw Data Results: Test data point M21

$\text{mean}(\text{Data}^{\langle 3 \rangle}) = -0.35653$	mean value
$\text{stdev}(\text{Data}^{\langle 3 \rangle}) = 22.19756$	standard deviation
$\max(\text{Data}^{\langle 3 \rangle}) = 70.05$	maximum
$\min(\text{Data}^{\langle 3 \rangle}) = -88.03337$	minimum

Plot of original data of SMT Raw Data M21

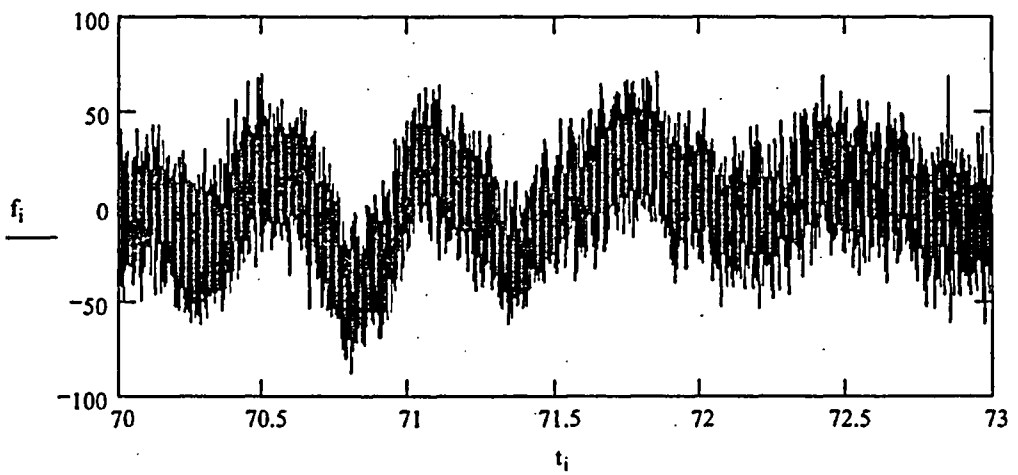

Plot of the magnitude of the fourier coefficients as a function of frequency SMT Raw Data M21

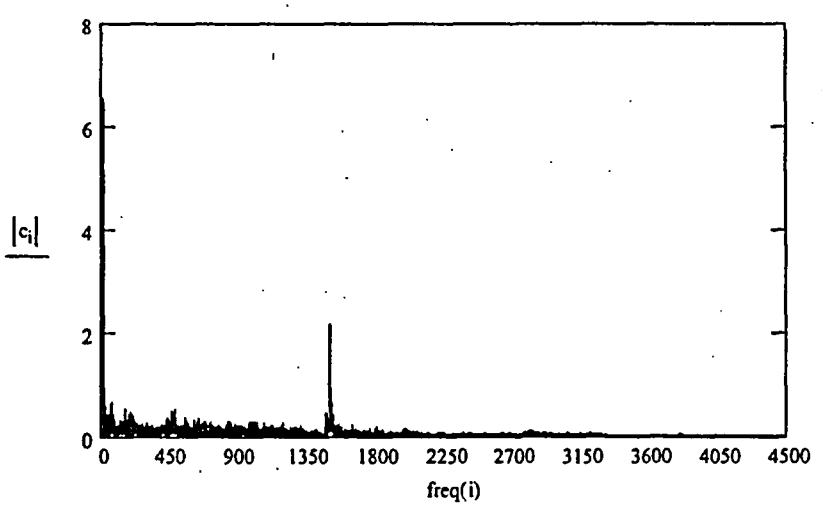

Appendix B

Power Spectral Density Plots of Filtered Test and Computed Data

Test data point M9

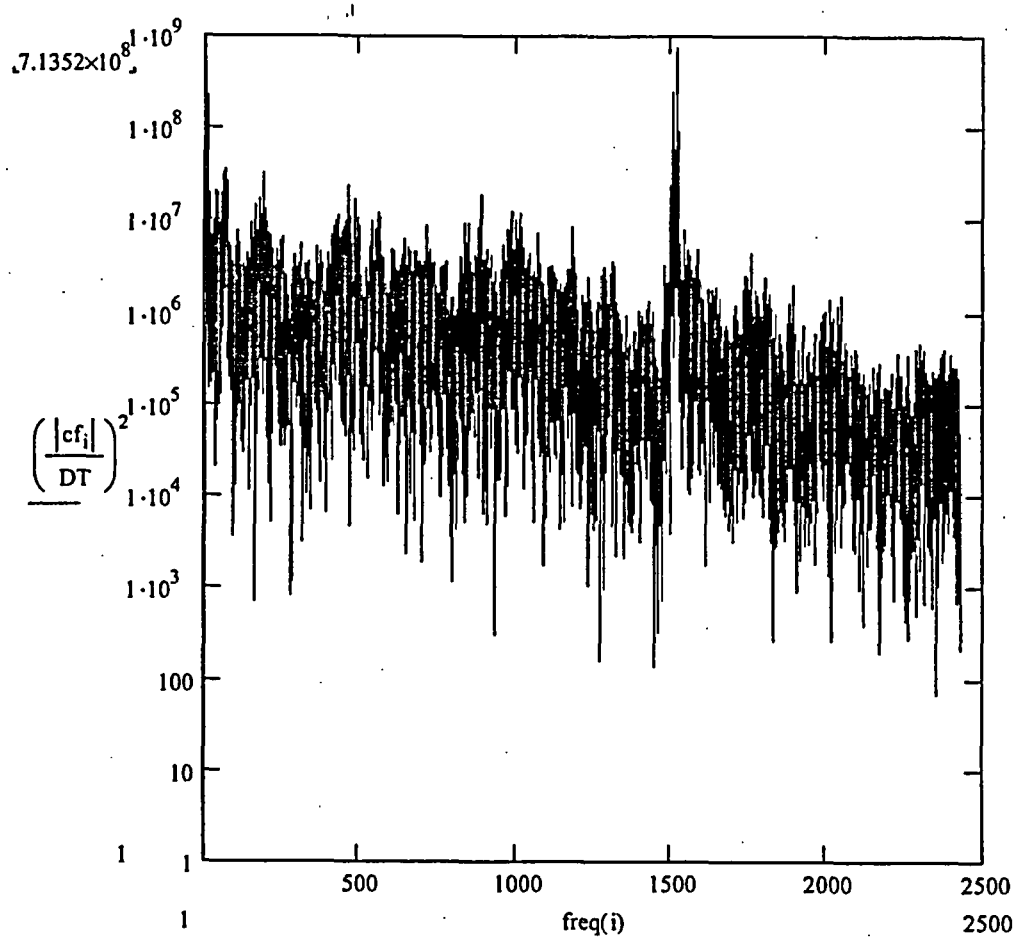

First Case Computation point M9

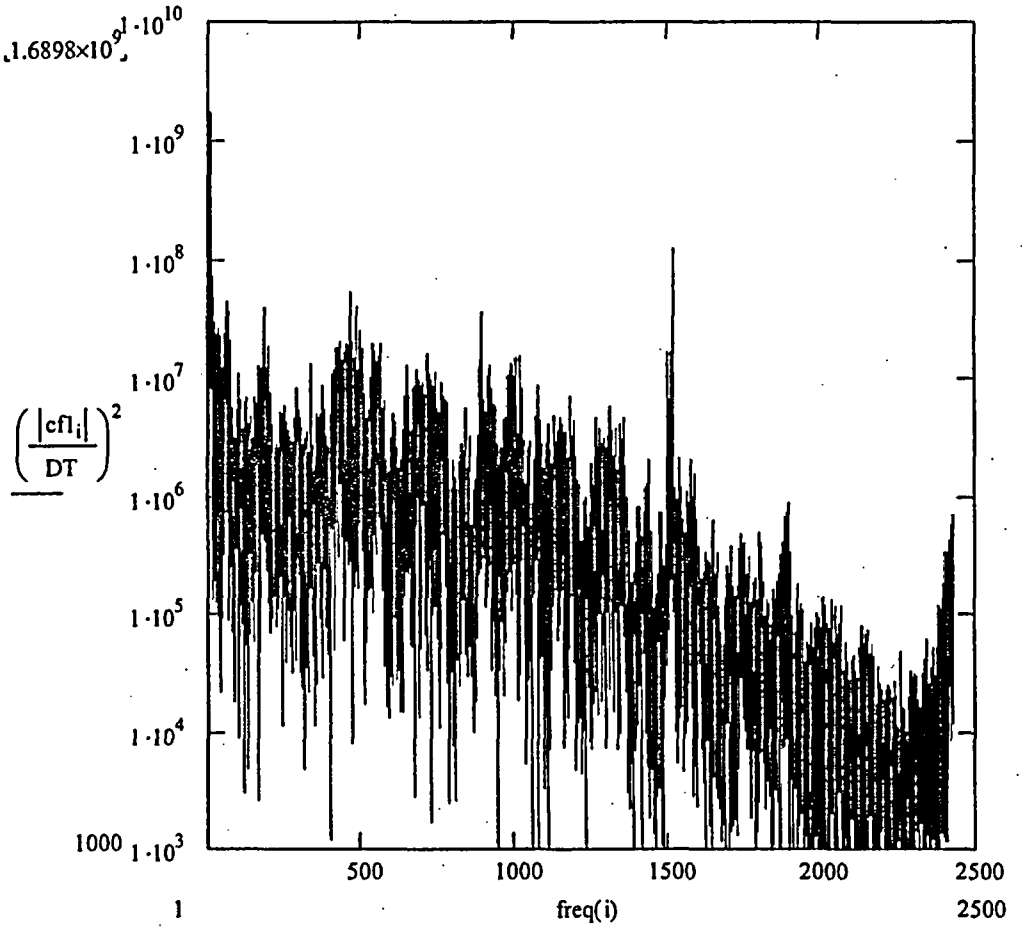

Second Case Computation point M9

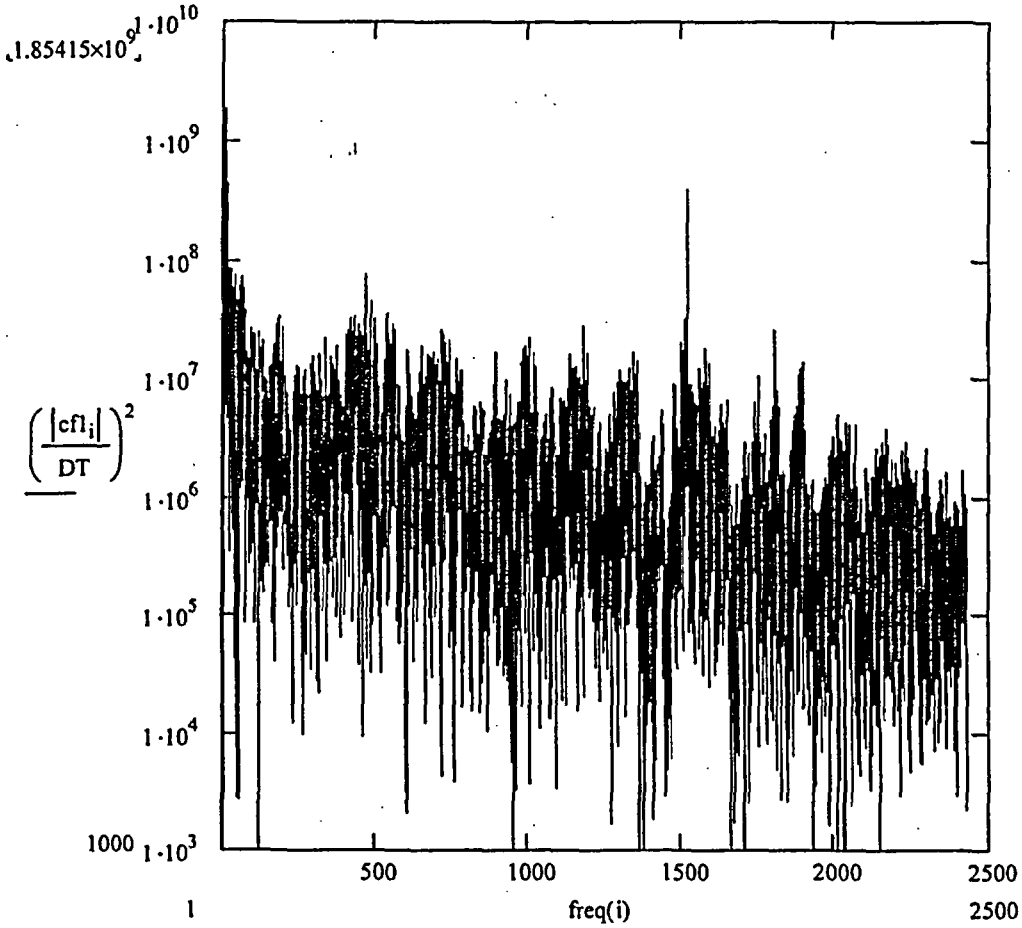

Test data point M21

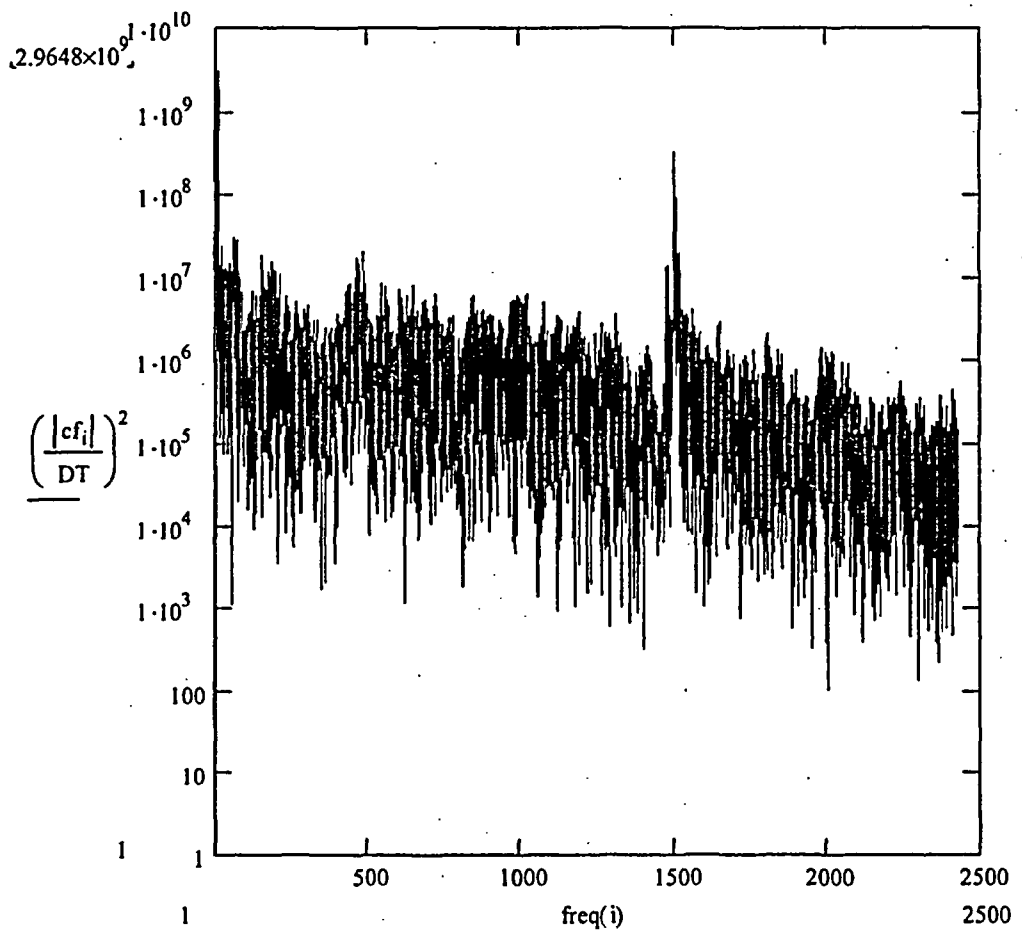

First Case Computation point M21

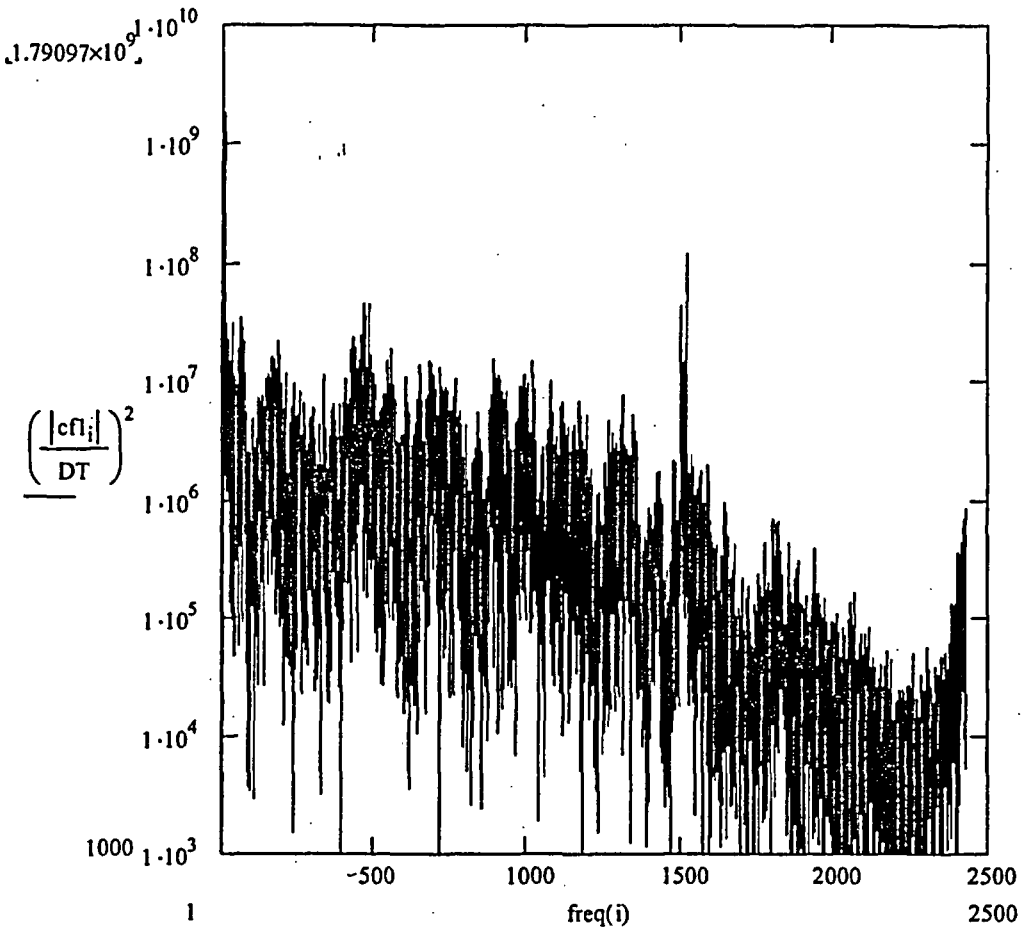

Second Case Computation point M21